TITLE PAGE

The Impact of the Alkyne Substitution Pattern and Metallation on the Photo-isomerization of Azobenzene-based Platinum(II) Di-ynes and Poly-ynes

Rayya A. Al-Balushi,[†] Ashanul Haque,[†] Maharaja Jayapal,[†] Mohammed K. Al-Suti,[†] John Husband,[†] Muhammad S. Khan,[*†] Jonathan M. Skelton,[*§] Kieran C. Molloy,[§] and Paul R. Raithby[*§]

[†]Department of Chemistry, Sultan Qaboos University, P.O. Box 36, Al Khod 123, Sultanate of Oman. E-mail:msk@squ.edu.om

[§]Department of Chemistry, University of Bath, Claverton Down, Bath BA2 7AY, UK. E-mail:j.m.skelton@bath.ac.uk, p.r.raithby@bath.ac.uk

Keywords: Azobenzene, Conjugation, Pt(II) acteylide complexes, Photoisomerization, time-dependent density-functional theory.

The Impact of the Alkyne Substitution Pattern and Metallation on the Photo-isomerization of Azobenzene-based Platinum(II) Di-ynes and Poly-ynes

Rayya A. Al-Balushi,[†] Ashanul Haque,[†] Maharaja Jayapal,[†] Mohammed K. Al-Suti,[†] John Husband,[†] Muhammad S. Khan,[*†] Jonathan M. Skelton,[*§] Kieran C. Molloy,[§] and Paul R. Raithby[*§]

ABSTRACT

Trimethylsilyl-protected di-alkynes incorporating azobenzene linker groups, $Me_3Si{-}C{\equiv}C{-}R{-}C{\equiv}C{-}SiMe_3$ (R = azobenzene-3,3'-diyl, azobenzene-4,4'-diyl**,** 2,5-bisoctylazobenzene-4,4'-diyl**),** and the corresponding terminal dialkynes, $H{-}C{\equiv}C{-}R{-}C{\equiv}C{-}H$, have been synthesised and characterized. The CuI-catalyzed dehydrohalogenation reaction between *trans*-$[Ph(Et_3P)_2PtCl]$ and the deprotected dialkynes in a 2:1 ratio in $^{i}Pr_2NH/CH_2Cl_2$ gives the Pt(II) di-ynes *trans*-$[Ph(Et_3P)_2Pt{-}C{\equiv}C{-}R{-}C{\equiv}C{-}Pt(PEt_3)_2Ph]$, while the dehydrohalogenation polycondensation reaction between *trans*-$[(^{n}Bu_3P)_2PtCl_2]$ and the dialkynes in a 1:1 molar ratio under similar reaction conditions affords the Pt(II) poly-ynes, $[{-}Pt(P^{n}Bu_3)_2{-}C{\equiv}C{-}R{-}C{\equiv}C{-}]_n$. The materials have been characterized spectroscopically, with the di-ynes also studied using single-crystal X-ray diffraction. The Pt(II) di-ynes and poly-ynes are all soluble in common organic solvents. Optical-absorption measurements show that the compounds incorporating the *para*-azobenzene spacer have a higher degree of electronic delocalisation than their *meta*-azobenzene counterparts. Reversible photoisomerization in solution was observed spectroscopically for the alkynyl-functionalised azobenzene ligands and, to a lesser extent, for the Pt(II) complexes. Complementary quantum-chemical modelling was also used to analyse the optical properties and the isomerisation energetics.

INTRODUCTION

With the rapidly-developing interest in molecular switches, a considerable amount of work is being carried out worldwide to identify suitable materials. Examples exist of molecular switching through both physical and chemical means,[1] and the materials have a wide range of applications including in optoelectronics, as holographic materials, and for multicolour displays and data-storage and communication technologies.[2] To achieve this switching functionality, many organic chromophore building-blocks such as stillbenes, azobenzenes, spiropyranes, fulgides, and chromenes are available and readily incorporated into more complex systems.[3] Of these, diazene or azo moieties are well-established and promising chromophores, being robust, chemically stable and cost effective.[4] Many new materials have been designed based on this chromophore, showing a range of novel properties.[2]

We have a long-standing interest in conjugated "rigid-rod" poly(metalla-ynes), which represent a class of solution-processable materials with tunable opto-electronic properties.[5] The rigid backbone of the poly-ynes facilitates extended electronic delocalization along the polymer chain, allowing for efficient electronic transport and thus enabling the compounds to function as molecular wires. Metallo poly-ynes have been used as model systems for the study of some of the photophysical processes that occur in the conjugated organic polymers used in organic light-emitting diodes (OLEDs),[6] lasers,[7] photovoltaic cells,[8] field-effect transistors (FETs),[9] surface acoustic-wave (SAW) sensors and non-linear optical (NLO) materials.[10] Incorporation of heavy metals such as Pt into the polymer backbone introduces large spin-orbit coupling effects, which allow for light emission from triplet excited states. Moreover, the role of the spacer group in the polymer structure is also well established,[11] with Pt(II) poly-ynes incorporating a wide range of conjugated aromatic and hetero-aromatic spacers having been investigated by us and by others.[12]

In this work, we have explored the synthesis and characterization of di- and poly(platina-ynes) incorporating both *meta* (*m*)- and *para* (*p*)-substituted azobenzene spacers. We have performed a comprehensive structural and spectroscopic characterization of nine materials, and elucidated how the substitution pattern on the spacer and complexation with platinum affects the absorption profile, highlighting the difference between the *meta* and *para* forms. The difference in the conjugation in the two series mirrors the difference in the electronic properties recently reported for the related di-platinum complexes linked by 2,7- and 3,6-carbazole-diyl units, where the carbazole-2,7-diyl units display enhanced conjugation.[13] Preliminary photoirradiation experiments on these di-platinum diynes indicate that the

spacers, and, to a lesser extent, the organometallic species, undergo reversible photoinduced *trans*-to-*cis* isomerisation about the azo bond in solution, as observed for closely related di-platinum diyl azobenzene linked complexes.[14] The experimental measurements are supported by quantum-mechanical modelling of a subset of the materials, which is used to interpret the spectroscopy and to investigate the energetics of the isomerisation.

RESULTS AND DISCUSSION

Synthesis and spectroscopic characterization

A slightly modified palladium(II)/copper(I)-catalyzed cross-coupling reaction between the diiodo azobenzenes **1-3** with trimethylsilylethynyl was performed in $^{i}Pr_2NH$/THF to obtain 1,2-bis(3-((trimethylsilyl)ethynyl)phenyl)diazene (**1a**), 1,2-bis(4-((trimethylsilyl)ethynyl)phenyl)diazene (**2a**) and 1,2-bis(2,5-dioctyl-4-((trimethylsilyl)ethynyl)phenyl)diazene (**3a**) (**Scheme 1**).[15] The protected di-alkynes (**1a**-**3a**) were found to be stable in air and light, and were fully characterized by infrared (IR) and NMR (^{1}H and ^{13}C) spectroscopy, electrospray ionization (ESI) mass spectrometry, and elemental analysis.

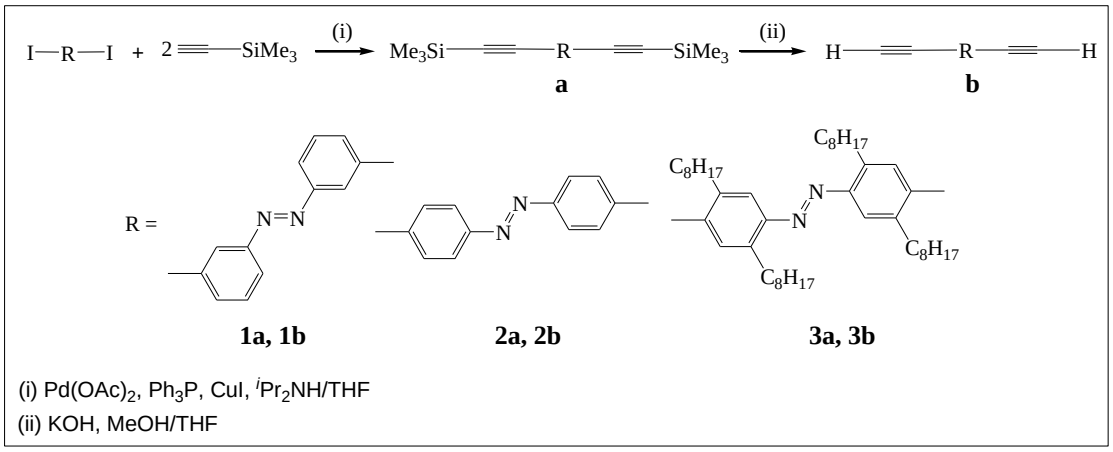

Scheme 1 Synthesis of bis(trimethylsilyl)-protected and diterminal-alkyne ligands incorporating azobenzene moieties.

Proto-desilylation of **1a**-**3a** was accomplished by cleavage of the trimethylsilyl groups with dilute aqueous KOH in MeOH/THF to generate the diterminal alkynes bis(3-ethynylphenyl)diazene (**1b**), bis(4-ethynylphenyl)diazene (**2b**) and 1,2-bis(4-ethynyl-2,5-dioctylphenyl)diazene (**3b**) under similar conditions to those reported previously for related systems.[12b, 12f, 16] The terminal di-alkynes **1b**-**3b** were purified by silica-gel column

chromatography, and were isolated as orange or brown solids with typical overall yields of between 76 and 91%. The synthesis and characterisation of compound **2b** has been reported previously.[14] These diterminal alkynes were found to be highly reactive, and were therefore freshly prepared before reaction with the Pt(II) precursor complexes.

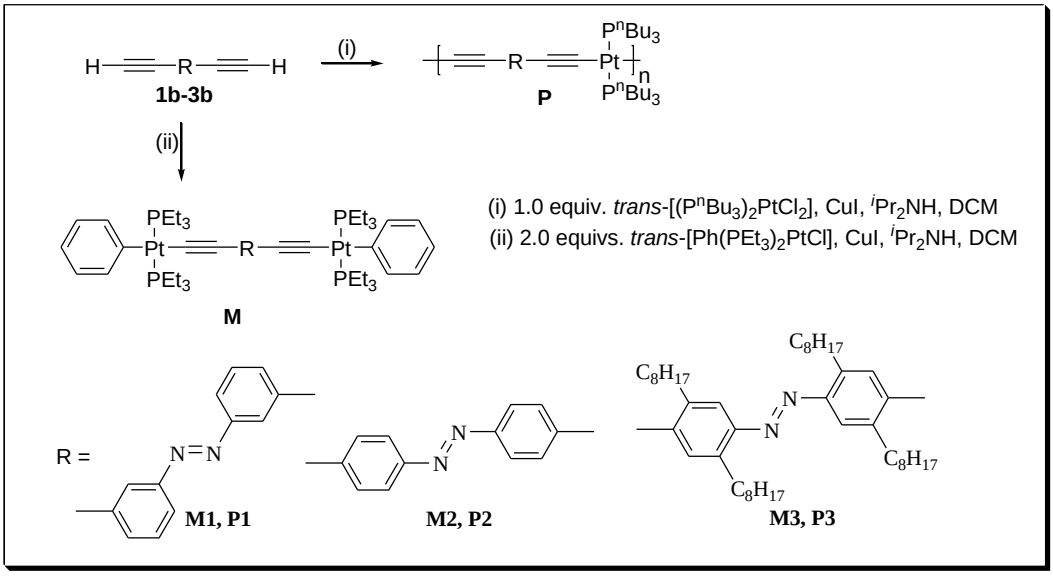

Scheme 2 Synthesis of Pt(II) di-ynes and poly-ynes incorporating azobenzene spacers.

The dehydrohalogenation reactions between *trans*-[(Ph(Et_3P)$_2$PtCl] and **1b**-**3b** in 2:1 stoichiometry, in $^{i}Pr_2NH/CH_2Cl_2$ in the presence of CuI at room temperature, afforded the Pt(II) di-ynes **M1**-**M3**, while the polycondensation reactions between *trans*-[($^{n}Bu_3P$)$_2$PtCl$_2$] and **1b**-**3b** in a 1:1 ratio under similar reaction conditions yielded the Pt(II) poly-ynes **P1**-**P3** (**Scheme 2**). Purification of the Pt(II) di-ynes and poly-ynes was carried out using silica and alumina columns, respectively. The Pt(II) poly-ynes were obtained in yields of 78-80%, indicating a very high conversion compared to the Pt(II) di-ynes which were obtained in 61-62% yield. The Pt(II) di-ynes and poly-ynes were fully characterized by UV-visible, IR and NMR spectroscopy, ESI mass spectrometry, and elemental analysis.

The IR spectra of the Pt(II) di-ynes **M1**-**M3** and the poly-ynes **P1**-**P3** show a single, sharp $\nu_{C\equiv C}$ absorption at 2090-2098 cm^{-1}, which is consistent with a *trans* configuration of the ethynylenic units around the Pt(II) center. The bond stretch frequency is similar to that found in a range of related materials.[12d, e] The $\nu_{C\equiv C}$ values for the terminal di-ynes **1b**-**3b** (2105-2109 cm^{-1}) are considerably lower than those of the corresponding trimethylsilyl-protected di-alkynes **1a**-**3a** (2152-2155 cm^{-1}), as is expected.[17] The Pt(II) di-ynes and poly-ynes display lower $\nu_{C\equiv C}$ values than those in the corresponding protected or terminal di-alkynes, an

observation which has been attributed to either metal-yne π backbonding, or to the $M^{\delta+}$-$C^{\delta-}$ polarity.[18]

In all the ligand precursors and Pt(II) complexes, clear ^{1}H NMR resonances from the protons of the aromatic ring systems were observed, indicating both the Pt(II) di-ynes and poly-ynes to be structurally rigid. The two distinct ^{13}C NMR resonances of the ethynylenic carbons in the di-ynes and poly-ynes were both shifted downfield relative to the signals from the diterminal alkynes, in agreement with the expected structures. The resonances due to the ethyl and butyl groups of the auxiliary ligands in the Pt(II) di-ynes and Pt(II) poly-ynes, respectively, could be clearly identified. The single resonance in the ^{31}P NMR spectra of the Pt(II) di-ynes and poly-ynes further confirms the *trans*-arrangement of the phosphine ligands. The $^{1}J_{Pt\text{-}P}$ values range from 2629-2654 Hz for the di-ynes to 2338-2347 Hz for the poly-ynes; these spectral features are similar to those of previously-reported Pt(II) di-ynes and poly-ynes,[12a, 12g] and again confirms the all-*trans* configuration around the metal centers.

The mass spectrometry results confirm the molecular masses expected for the ethynyl ligands and the Pt(II) di-yne complexes. Gel-permeation chromatography (GPC), calibrated against a polystyrene standard, gave weight-average molecular weights (M_w) for the poly-ynes **P1**-**P3** in the range of 41,800–84,400 g/mol, corresponding to degrees of polymerization (DPs) between 35 and 55. The polydispersity index (PDI) was found to vary between 1.2 and 1.4. The relatively narrow polydispersity (PDI < 2) in the molecular weights is consistent with the proposed linear structure from the condensation polymerisation. However, the absolute molecular weights determined by GPC should be treated with caution; GPC provides a measure of hydrodynamic volume, which is different for rigid-rod and flexible polymers. Thus, the M_w values determined by this technique using the polystyrene standard are likely to artificially increase the measured molecular weights to some extent. However, high degree of polymerization in the poly-ynes was supported by NMR spectroscopy in which resonances corresponding to protons on the terminal end groups were too weak to be observed.

Structural characterization

In addition to the spectroscopic characterization, we were also able to grow crystals of the Pt(II) di-yne complexes **M1** and **M2** which were suitable for single-crystal X-ray diffraction. The key crystallographic data is summarized in **Table 1**, and images of the two structures are shown in **Figures 1** and **2**.

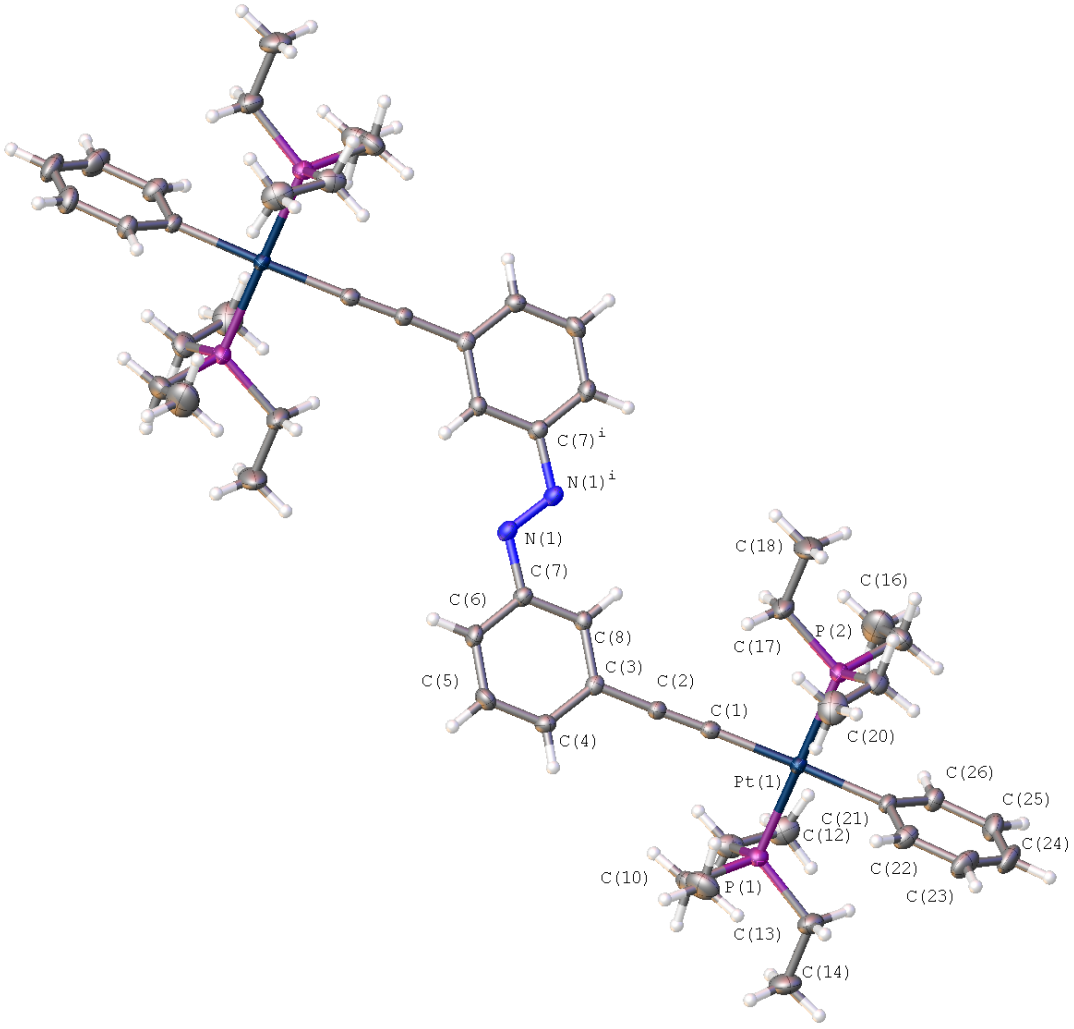

Figure 1 Crystal structure of **M1**, with the unique atoms numbered as shown. Displacement ellipsoids are plotted at the 50% probability level. Selected geometric data: C(1)-Pt(1) 2.017(3) Å, C(21)-Pt(1) 2.069(3) Å, P(1)-Pt(1) 2.2882(7) Å, P(2)-Pt(1) 2.2856(7) Å, C(1)-C(2) 1.212(4) Å, C(2)-C(3) 1.439(3) Å, N(1)-N(1^{i}) 1.246(4) Å, ∠C(1)-Pt(1)-C(21) 176.06(11) º, ∠C(1)-Pt(1)-P(1) 87.42(7) º, ∠C(1)-Pt(1)-P(2) 92.27(8) º, ∠C(21)-Pt(1)-P(1) 92.27(8) º, ∠C(21)-Pt(1)-P(2) 88.19(8) º, ∠P(2)-Pt(1)-P(1) 179.01(3) º, ∠C(2)-C(1)-Pt(1) 174.2(2) º, ∠C(1)-C(2)-C(3) 176.7(3) º, ∠N(1^{i})1-N(1)-C(7) 114.6(3) º. Symmetry operation (^{i}): *-x*, 1 - *y*, *-z*.

Table 1 Crystallographic data for **M1** and **M2**.

	M1	**M2**
CCDC code	1486091	1486092
Empirical formula	$C_{52}H_{78}N_2P_4Pt_2$	$C_{52}H_{78}N_2P_4Pt_2$
Formula weight / amu	1245.22	1245.22
Temperature / K	150(2)	250(2)
Crystal system	Monoclinic	Triclinic
Space group	$P2_1/c$	P-1
a / Å	18.7794(4)	8.9899(3)
b / Å	10.5232(2)	9.6169(3)
c / Å	14.8114(3)	15.8333(7)
α / °	90.0	92.353(3)
β / °	110.929(3)	93.954(3)
γ / °	90.0	94.633(3)
V / Å^3	2733.89(11)	1359.65(9)
Z	2	1
ρ_{calc} g cm^{-3}	1.513	1.521
μ / mm^{-1}	5.262	5.290
F(000)	1240	620
Crystal size / mm^3	0.35 × 0.30 × 0.15	0.34 × 0.19 × 0.04
Radiation	MoKα (λ = 0.71073 Å)	MoKα (λ = 0.71073 Å)
2θ range for data collection / °	6.732 - 61.958	5.96 - 61.02
Index ranges	$-26 \le h \le 26$, $-14 \le k \le 15$, $-20 \le l \le 21$	$-12 \le h \le 12$, $-13 \le k \le 13$, $-22 \le l \le 22$
Reflections collected	70107	23252
Independent reflections	8186 [R_{int}= 0.0495, R_{sigma}= 0.0329]	8278 [R_{int}= 0.0363, R_{sigma}= 0.0433]
Data/restraints/parameters	8186 / 0 / 277	8278 / 51 / 334
Goodness-of-fit on F^2	1.060	1.042
Final R indexes [I>=2σ (I)]	R_1= 0.0287, wR_2= 0.0508	R_1= 0.0397, wR_2= 0.0809
Final R indexes [all data]	R_1= 0.0396, wR_2= 0.0533	R_1= 0.0545, wR_2= 0.0879

M1 crystallises in the monoclinic space group $P2_1/c$, with half a dimeric complex in the asymmetric unit and the midpoint of the azo N=N bond corresponding to a crystallographic center of symmetry. The crystal structure is shown in **Figure 1**, and confirms the *trans* conformation about the azo bond in the spacer group, the *meta* substitution of the arene rings on the spacer, and the *trans* arrangement of the phosphine ligands on the square-planar Pt(II) centers. We observed no significant short intermolecular contacts within the crystal structure, with the dimeric complexes all being separated by normal van der Waals' distances.

The crystallographic symmetry implies that the azobenzene spacer, which forms the central core of the complex, i.e. the Pt-C≡C-*m*-C_6H_4-N=N-*m*-C_6H_4-C≡C-Pt unit, is planar. The coordination geometry around each of the two Pt(II) centers is, as noted above, square

planar; the terminal phenyl rings are at an angle of 86.90 ° with respect to the unique Pt(II) coordination plane, and the plane is itself at an angle of 37.86 ° with the phenyl ring of the azobenzene spacer. All other bond parameters were found to be within the expected ranges for dimeric Pt(II) diyne complexes.[11-12]

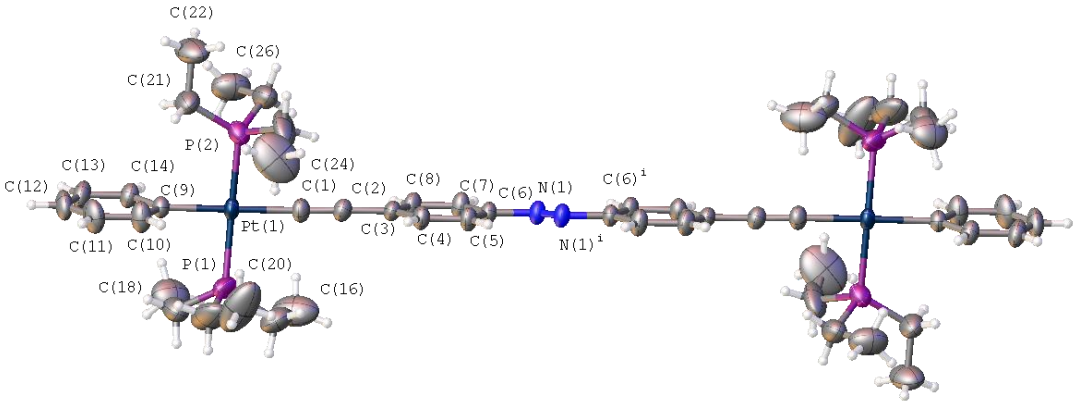

Figure 2 Crystal structure of **M2**, with the unique atoms numbered as shown. Displacement ellipsoids are plotted at the 50% probability level. Selected geometric data: C(1)-Pt(1) 2.018(4) Å, C(9)-Pt(1) 2.062(4) Å, P(1)-Pt(1) 2.2938(14) Å, P(2)-Pt(1) 2.2851(13) Å, C(1)-C(2) 1.207(6) Å, C(2)-C(3) 1.441(6) Å, N(1)-N(1^{i}) 1.254(7) Å; ∠C(1)-Pt(1)-C(9) 178.69(17) º, ∠C(1)-Pt(1)-P(2) 87.55(14) º, ∠C(1)-Pt(1)-P(1) 92.62(14) º, ∠C(9)-Pt(1)-P(1) 88.16(12) º, ∠C(9)-Pt(1)-P(2) 91.56(12) º, ∠P(2)-Pt(1)-P(1) 173.87(6) º, ∠C(2)-C(1)-Pt(1) 177.3(4) º, ∠C(1)-C(2)-C(3) 177.7(5) º, ∠N(1^{i})1-N(1)-C(6) 114.1(4) º; symmetry operation (^{i}): 2 - *x*, 2 - *y*, -*z*.

M2 crystallises in the lower-symmetry triclinic space group *P*-1 (**Figure 2**). As in the **M1** structure, the asymmetric unit contains half a molecular complex, with the midpoint of the N=N double bond located on a crystallographic center of symmetry. The X-ray structure confirms the *trans* geometry about the azo bond in the spacer group, the *para* substitution of the spacer arene rings, and the square-planar coordination of the metal, with a *trans* relationship between the phosphine ligands. Again, there are no significant short intermolecular contacts less than the sum of the van der Waals radii.

As in the structure of **M1**, the phenyl rings in the azobenzene group are coplanar. In contrast, however, the dihedral angle between the unique arene ring and the Pt(II) square plane is 86.77 °, compared to the equivalent angle 37.86 ° in **M1**. The angle between the Pt(II) coordination plane and the terminal phenyl ring is 86.89 °, making it is almost coplanar with the arene ring of the azobenzene spacer, as opposed to almost perpendicular to it as in **M1**. Since within the molecule there is free rotation about the Pt-C bond connecting the

spacer and the Pt(II) center, it is not surprising that there is considerable variation in the dihedral angle between the central spacer and the Pt(II) coordination plane. Although there is variation in the angle of the terminal phenyl ring with respect to the phenyl rings in the spacer group, in both structures the terminal phenyl rings sit perpendicular to the Pt(II) plane, as is typically found to be the case in dimeric diplatinum diyne complexes of this type. The intramolecular bond parameters in **M2** are similar to those in **M1**, and in related dinuclear diplatinum complexes. [11-12]

Optical-absorption spectroscopy

The room temperature solution absorption spectra of the Pt(II) di-ynes (**M1-M3**) and Pt(II) poly-ynes (**P1-P3**) in CH_2Cl_2 are shown in **Figure 3**.

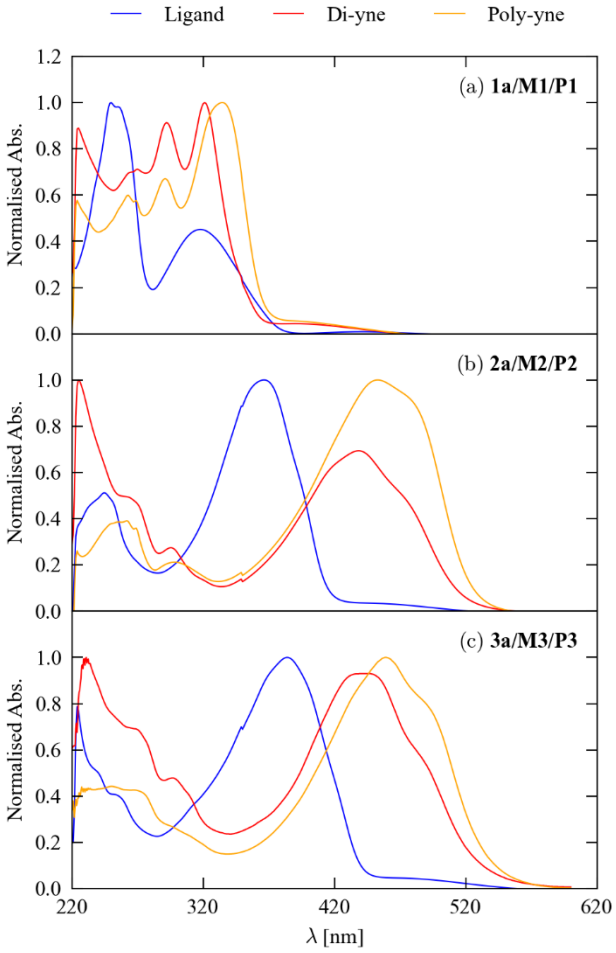

Figure 3 Normalized solution UV-visible absorption spectra of the protected ligands **1a**-**3a** and the corresponding Pt(II) di-ynes **M1**-**M3** and poly-ynes **P1**-**P3** in CH_2Cl_2.

The spectra of the protected ligands show intense primary absorption bands at ~320 (**1a**), 370 (**2a**) and 390 nm (**3a**), which were assigned as π->π* transitions, together with weaker absorptions at longer wavelength which are ascribed to weak *n*->π* transitions.[19]

For the Pt(II) di-ynes and poly-ynes of **2a** and **3a** (**M2**/**M3** and **P2**/**P3**, respectively; **Figures 3b**/**3c**), there is a clear red shift in the absorption profile compared to the corresponding protected ligands. The absorption maxima in the spectra of the di-ynes **M2** and **M3** occur at ~440 nm, while the maxima in the spectra of the corresponding poly-ynes **P2** and **P3** are further red shifted to approx. 460 nm. All four spectra also appear to exhibit a prominent longer-wavelength shoulder feature, leading to a significantly enhanced absorption out to ~500-550 nm compared to the protected ligands.

The fact that there is a red shift in the spectra of both **P2** and **P3** compared to the di-yne Pt(II) complexes (**M2** and **M3)** suggests enhanced electronic delocalisation along the polymer chains, which would require conjugation through the Pt(II) centers. That such conjugation is possible, which was confirmed by supporting calculations (see **Computational modelling** section). The enhanced absorption at visible wavelengths can, as in related materials, be attributed to metal-to-ligand charge-transfer (MLCT) excitations.[20]

In contrast, the trend for **M1** and **P1** (**Figure 3a**) is markedly different. In the absorption profiles of **M1** and **P1**, the long-wavelength maxima occur at ~320 and 335 nm, respectively, which are substantially blue shifted compared to the maxima of the other di-ynes and poly-ynes. The bands also appear to have a considerably narrower bandwidth than the corresponding features in the spectra of the other Pt(II) species. Either or both of these observations may be related to the alkyne groups in the azobenzene spacer in the **M1**/**P1** series being *meta* to the azo bond, as opposed to *para* in the **M2**/**P2 and M3**/**P3** series.

Photo-irradiation

Azobenzenes are well known for their ability to show *cis-trans* isomerisation following thermally- or photo-induced excitation.[21] The resultant large geometric change can potentially be harnessed for a number of applications including liquid crystals,[22] molecular photoswitches,[23] and photochromic ligands for optochemical genetics.[24] The isomerisation of the azobenzene-containing materials depends on several factors, including the chemical structure (e.g. to what extent the isomerisation is restricted by steric constraints), the degree of conjugation, and the influence of the solvent.[25]

We therefore performed preliminary photo-irradiation experiments on the **1a** and **2a** series of compounds, with these six materials being chosen in order to examine the effects of

the alkyne groups being *para* or *meta* to the azo bond. A series of experiments were performed in which CH_2Cl_2 solutions of **1a**, **2a**, and the corresponding Pt(II) di-ynes and poly-ynes (**M1**/**M2** and **P1**/**P2**, respectively) were irradiated with a 254 nm UV lamp (6 W) for 60 min, and the isomerisation followed spectroscopically by recording UV/visible spectra at ten-minute intervals. Although the spectra possess features at longer wavelengths, we found that we were only able to observe spectral changes at this wavelength. To check for the recovery of spectral changes induced by the UV irradiation, following the experiments the solutions were allowed to stand in ambient light for at least 48 h, and a final spectrum recorded to compare against the time zero measurement. The recorded time series are shown in **Figures 4**.

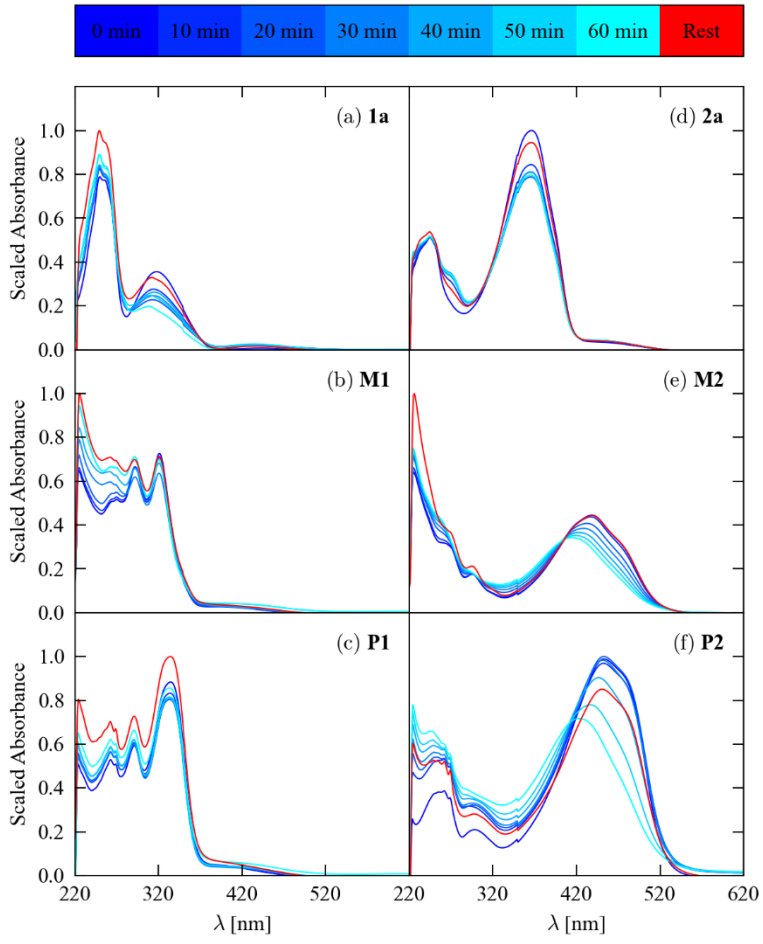

Figure 4 Time evolution of the UV-visible absorption spectra of the trimethylsilyl-protected azobenzene ligands **1a** and **2a** (a, d) and the corresponding Pt(II) di-ynes **M1** and **M2** (b, e) and poly-ynes **P1** and **P2** (c, f) in CH_2Cl_2 under irradiation with 254 nm UV light. The red lines, marked "Rest" on the colour scale, are spectra recorded after leaving the solutions stood in ambient light for minimum of 48 h, to check for the recovery of the spectral features after the photoirradiation experiment.

The series of spectra of the protected ligands in **Figures 4a** and **4d** show consistent spectral changes as a function of irradiation time, with a fall in the intensity of the primary absorption bands at 320 and 370 nm together with a corresponding growth in a shorter-wavelength feature. With reference to the simulated spectra in the ***Computational modelling*** section, these changes can be ascribed to the formation of the *cis* isomers. While the time series thus indicate that both protected ligands undergo photoinduced isomerisation, the spectral changes appear to saturate at long irradiation times, suggesting that the photochemical conversion does not go to completion.

Whereas **1a** shows significant photoisomerization, the spectral changes in the absorption profiles of **M1** and **P1** are rather less marked, with the main spectral change being a growth in the short-wavelength part of the absorption profile. With reference to the calculations, the two absorption maxima at 323 and 295 nm in the spectrum of **M1** might be attributable to the *cis* and *trans* isomers of this complex, which would suggest that a small amount of photoisomerization occurs under UV irradiation. There is also a similar trend visible in the spectra of **P1**, although it is not clear whether this can be attributed to an increase in the proportion of *cis* spacer units in the polymer backbone. Presuming it can, the changes are less marked than in the spectrum of **M1**, which would suggest that isomerization happens less readily in the polymer than in the di-yne complex.

In contrast, the spectra of the Pt(II) species incorporating **2a**, *viz.* **M2** and **P2**, do appear to undergo systematic changes under UV irradiation, with a blue shift and a decrease in intensity of the prominent absorption bands at ~440 and 460 nm. Energetics calculations (see the ***Computational modelling*** section) suggest that the *cis*-azo form of **M2** is more energetically unfavourable than the corresponding isomer of **M1**, and, of course, both are considerably less stable than the respective *trans* configurations; from this, one might infer that the apparently more facile isomerization of **M2** is due to stronger absorption and/or a more efficient coupling of the electronic excitations to the vibrational modes that effect the rearrangement. We also note that, in contrast to the spectra of the other species, the spectrum of **M2** has a clear isobestic point at ~420 nm, although the significance of this feature in the present context, and of the absence of similar features in the spectra of the other compounds, is not clear.

For **1a**, **2a**, **M1** and **M2**, the spectral changes are largely reversible under ambient conditions, with the absorption profiles of both solutions recorded after resting for >48 h being very similar to the time-zero spectra. On the other hand, the spectra of **P1** and **P2** recorded after 48 h differ more markedly from the time-zero measurements. However, we do

not observe the formation of new bands, as would be expected from sample degradation, and we found that longer irradiation of the solutions did indeed give rise to persistent new absorption peaks. Thus the origin of the difference between the spectra before the experiment and after resting could be due to small amounts of degradation, but might also be due to a drift in the spectrometer calibration and/or slow evaporation of the solvent during the experiment. In particular, the latter could explain the increased absorption of **1a** and **P1** after resting.

To check for possible influences of the solvent, we performed a second set of experiments in toluene (**Figure S1**), which was chosen for its lower polarity despite its strong absorption below ~280 nm. Bearing in mind the loss of signal at short wavelengths due to absorption from the solvent, the spectra of **1a**, **M1** and **P1** in toluene are fairly similar to those recorded in CH_2Cl_2, both in the shape and positions of the spectral bands (c.f. **Figure 3a** and **Figures 4a**-**4c**). The longest-wavelength absorption maxima in the profiles of **1a**/**M1** and **P1** occur at approx. 320 and 330 nm in toluene, respectively, which are very similar to the values in CH_2Cl_2. The progressive reduction in the intensity of the 320 nm absorption band on irradiation in the spectrum of **1a** again provides clear evidence for photoinduced isomerization. The spectra of **M1** and **P1** also display the same changes under illumination as in CH_2Cl_2. The changes are again much less marked than for **1a**, which suggests that isomerization in the Pt(II) species may be restricted.

Whereas the time series of **2a** appears to demonstrate similar behaviour to the spectra recorded in CH_2Cl_2, **M2** and **P2** appear to undergo very little change under irradiation in toluene. Although this could be taken to imply that the isomerization of these Pt(II) species is sensitive to the solvent, it could also be due simply to the strong absorption of toluene below 280 nm attenuating the excitation lamp. In this regard, we note that our energetics calculations do not predict the solvent to have a strong effect on the energy difference between the isomers of **M2**, and so a large difference in behaviour with respect to the experiments in CH_2Cl_2 would be unexpected. Comparing the spectra of **P2** in the two solvents, there appears to be a notable change to the relative magnitude of the signals forming the primary absorption bands, the origin of which is unclear.

To summarize, these photoisomerization experiments provide evidence that both ethynyl-functionalized *meta*- and *para*-azobenzene ligands display photoinduced *trans*-to-*cis* isomerization in solution, and that the photochemical switching may also be retained in the Pt(II) di-ynes and poly-ynes, albeit with a low photoisomerisation yield. The switching of the *para*-substituted azobenzene complexes appears to be more facile than that of the *meta*-

substituted analogues, which we suggest may be due to more efficient absorption and/or vibronic coupling in the former. The experiments provide little evidence for solvent effects, although we cannot draw any firm conclusions here based on the present results. While these preliminary studies suggest that the di-ynes and poly-ynes may show interesting photoisomerisation behaviour, more quantitative studies would need to be carried out to investigate this further, e.g. to test cycleability or to explore solvent effects in more detail. This is beyond the scope of the present study.

Computational modelling

In order to better understand the isomerisation behaviour and optical properties of the azobenzene ligands and the dinuclear Pt(II) complexes, we carried out computational modelling on the *cis* and *trans* forms of the deprotected ligands **1b** and **2b** and the corresponding model complexes **M1** and **M2** using hybrid density-functional theory (DFT).

Initial models of the *trans* conformations of **M1** and **M2** were made from the X-ray structures, while models of the *cis* configurations were prepared by manually rotating about the azo bond. Models of **1b** and **2b** were generated from the models of the Pt(II) complexes. Geomerty optimization was performed in the gas phase, and also using the COSMO solvation model[26] to mimic the dielectric environments of the solvents in which the spectra were recorded and the photoisomerization experiments performed, *viz.* CH_2Cl_2 (ε = 8.93) and toluene (ε = 2.38). Based on our findings, we also carried out further COSMO calculations with the higher dielectric constant of H_2O (ε = 80.1). To confirm the stability of the structures, particularly the four *cis* ones, we computed the nuclear Hessians of the gas-phase models, and observed no imaginary modes, indicating all eight to be energetic minima.

The four optimized gas-phase molecular models of the Pt(II) complexes are shown in **Figure 5**, and the calculated isomerisation energies of **1b**, **2b**, **M1** and **M2**, in the gas phase and in the three solvent continuua, are summarized in **Table 2**.

From these energetics calculations, it can be seen, as is expected, that for both substitution patterns the *cis* form of the azobenzene is consistently higher in energy than the *trans* configuration, both in the ligands and in the Pt(II) complexes, in agreement with the spectroscopic and structural characterization.

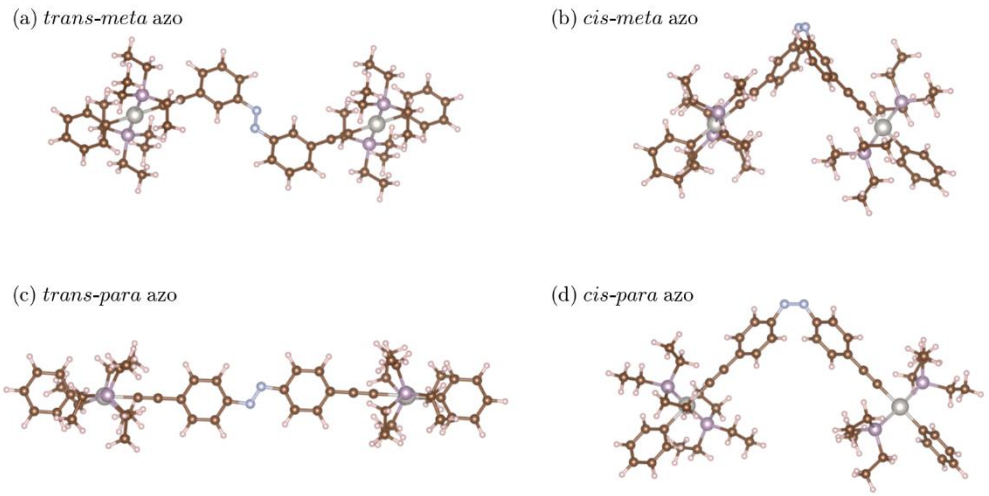

Figure 5 Optimised gas-phase geometries of Pt(II) di-yne complexes with the *meta*- (a, b; **M1**) and *para*-substituted (c, d; **M2**) azobenzene spacers in the *trans*- (a, c) and *cis*-azo (b, d) configurations. These images were generated with the VESTA software.[27]

Table 2 Calculated isomerisation energies $\Delta E_{cis\text{-}trans}$ of the *meta*- and *para*-substituted azobenzene spacer ligands **1b** and **2b** and the corresponding Pt(II) di-yne complexes **M1** and **M2**, after optimization in the gas phase and with the COSMO solvation model[26] using the dielectric constants of toluene, CH_2Cl_2 and H_2O.

	$\Delta E_{cis\text{-}trans}$ / kJ mol^{-1}			
	1b	**M1**	**2b**	**M2**
Gas phase	63.35	64.28	64.83	71.39
Toluene (ε = 2.38)	57.71	59.39	59.86	71.42
CH_2Cl_2 (ε = 8.93)	54.26	54.19	56.49	72.21
H_2O (ε = 80.1)	53.02	55.07	55.32	73.39

In the gas phase, the differences are 63.35 and 64.83 kJ mol^{-1} for the *meta*- and *para*-azo ligands **1b** and **2b**, respectively. These are on the same order as those calculated for azobenzene itself.[28] The energy difference for the *meta*-azo Pt(II) complex is similar at 64.28 kJ mol^{-1}, whereas that for the *para*-azo complex is ~10 % higher at 71.39 kJ mol^{-1}. This implies that the *cis* configuration of the *para*-azo complex is less favorable than that of the *meta*-azo one, presumably due to greater steric strain in the former.

The presence of a dielectric continuum significantly reduces the energy difference between the two isomers of **1b** and **M1**, by up to around 15 %, although in all cases the *cis* isomer remains higher in energy than the *trans* confuguration by a considerable margin. A

similar trend is observed for **2b**, whereas the presence of a continuum has comparatively little effect on the energy differences in the corresponding Pt(II) complex **M2**.

Taken as is, these results suggest that both **1b** and **2b** would show similar isomerization behavior, whereas the *meta*-azo complex **M1** might show more facile photoisomerization than the *para*-azo **M2**. However, these energetics calculations do not predict the activation barriers for the photochemical reactions, the energy differences are all considerably lower than the energy of a visible/UV photon, and the ease of isomerization will depend strongly on both the absorption strength and the coupling of the electronic excited states to the vibrations which effect to the change in geometry. As noted above, this may explain the apparently opposing trend seen for **M1** and **M2** in the photoisomerization experiments. There have also been reports in the literature that the presence of MLCT excitations can in some cases block photo-induced isomerization in azobenzene-containing transition-metal complexes.[29] ()

To investigate the electronic structure and optical properties of the spacers and complexes, time-dependent DFT (TD-DFT) calculations[30] were carried out on the CH_2Cl_2-optimised models, with the same dielectric continuum present to mimic the conditions under which the absorption profiles were measured.

The simulated absorption spectra of the *cis* and *trans* isomers of **1b** and **2b** are compared to the measured profiles of **1a** and **2a** in **Figure 6**, and the electronic excitations giving rise to the main absorption features are tabulated in **Table S1**. Given the assumed constant peak broadening of 0.2 eV, the agreement between the calculated and measured spectra is good, with a small degree of offset that can be ascribed to approximations in the TD-DFT method used in the calculations.

From the calculations, the *trans* forms of both azobenzenes give rise to strong absorption bands between ~300 and 450 nm. The absorption in **1b** is formed of two transitions involving the frontier highest-occupied and lowest-unoccupied molecular orbitals (HOMO/LUMO) and the lower-lying HOMO-3, leading to an asymmetric peak shape. The primary absorption band of **2b**, on the other hand, is due to the HOMO -> LUMO excitation, and the HOMO-3 orbital contributes to a much weaker excitation at 315 nm.

The HOMO -> LUMO transitions in the *cis* isomers are lower in energy, both being above 450 nm, but have much smaller oscillator strengths. In *cis*-**1b**, the HOMO-3 -> LUMO transition produces a comparatively strong absorption at 298 nm, while in *cis*-**2b** a collection of transitions from the HOMO-3, HOMO-2 and HOMO-1 produce an asymmetric band between ~300 and 350 nm.

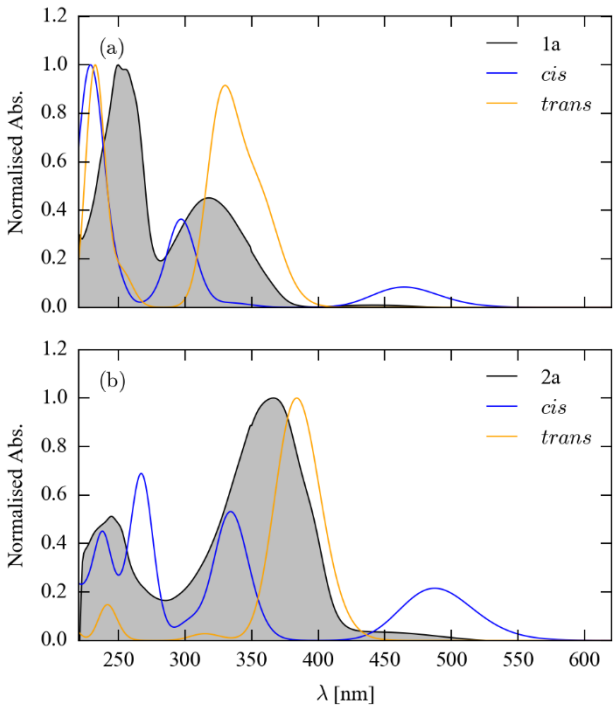

Figure 6 Simulated absorption spectra of the *meta*- and *para*-alkynyl azobenzene ligands **1b** (a) and **2b** (b) in the *cis*- (blue) and *trans*-azo (orange) configurations using time-dependent density-functional theory (TD-DFT). The experimental spectra of **1a** and **2a**, which are expected to possess comparable features, are overlaid as shaded black curves. All simulations were carried out using the COSMO solvation model[26] to mimic a solvent of CH_2Cl_2, as was used when measuring the experimental spectra.

These calculations help to account for the spectral changes observed in the photoisomerisation experiments carried out in CH_2Cl_2 (**Figure 4a**/**d**): an increase in the proportion of the *cis* isomer of **1a** should produce a reduction in intensity and a blue shift of the band centred around 320 nm, whereas the most prominent changes for **2a** are predicted to be a reduction in the intensity of the primary absorption band and the appearance and growth of a peak in the shoulder of the asymmetric feature around 250 nm.

The major difference between the simulated spectra of the *cis* and *trans* isomers of **M1** and **M2** (**Figure 7 a**-**d**) and those of the ligands in **Figure 6** can be surmised as a red shift of the most prominent absorption features, which is again consistent with the conclusions drawn from the spectroscopy.

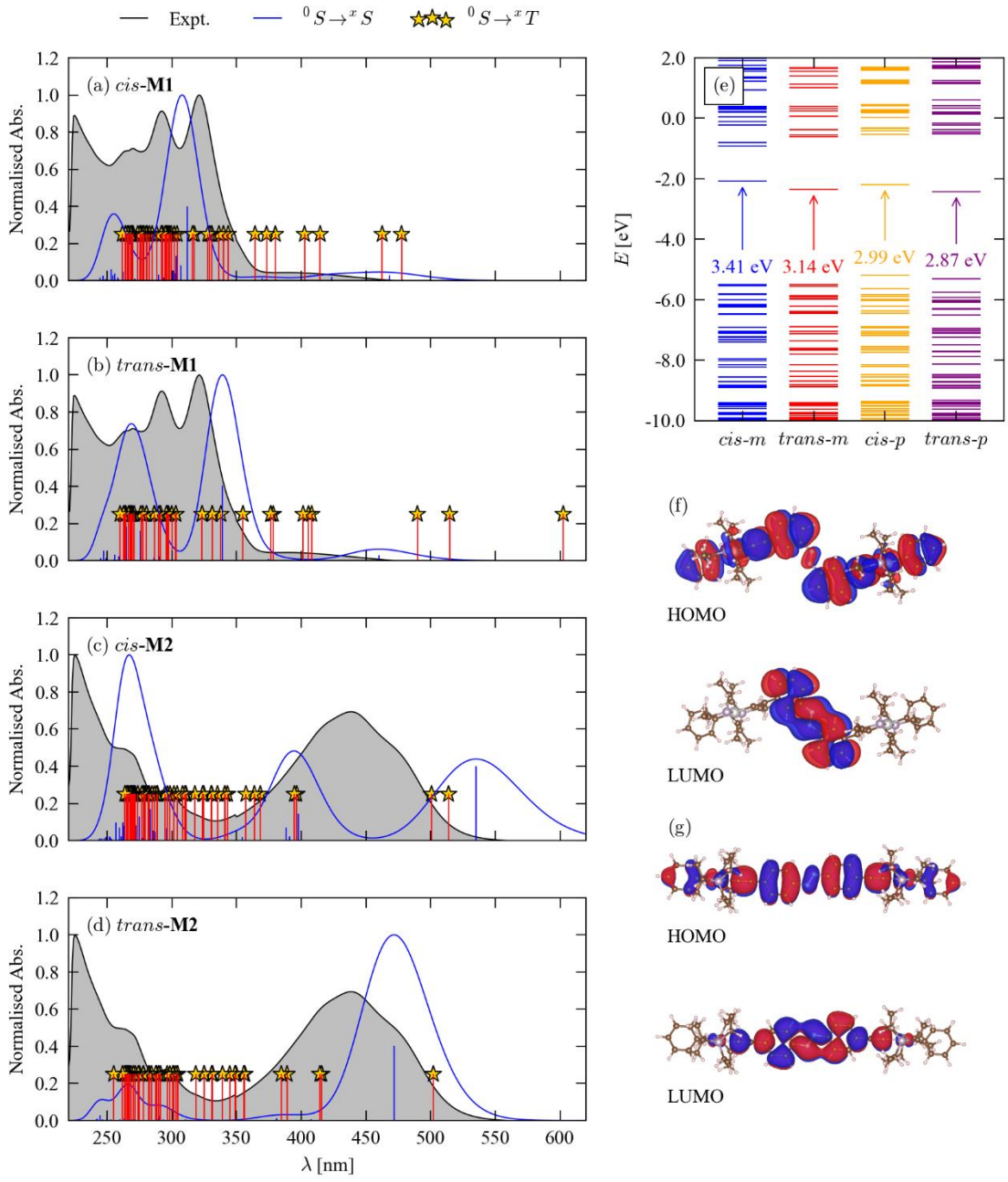

Figure 7 Electronic structure and optical properties of Pt(II) di-yne complexes with the *meta*- and *para*-substituted azobenzene spacers in the *cis*- and *trans*-azo configurations. (a-d) Simulated absorption spectra from time-dependent density-functional theory (TD-DFT) calculations (blue) compared to solution absorption spectra of **M1** (a, b) and **M2** (c, d). The vertical blue lines and red lines/gold stars indicate the positions of singlet and triplet excitations, respectively. (e) Electronic energy levels in the vicinity of the gap between the highest-occupied and lowest-unoccupied molecular orbitals (HOMO/LUMO), with the gaps as marked. (f, g) Frontier orbitals of *trans*-**M1** and *trans*-**M2**, respectively. All simulations were carried out using the COSMO solvation model[26] to mimic a solvent of CH_2Cl_2, as was used when measuring the experimental spectra.

A comparison of the oscillator strengths of the main transitions giving rise to the absorption bands (**Table S2**) suggests that the oscillator strengths in the Pt(II) complexes are enhanced, again as observed in the experiments. The major excitations in the *trans* forms of both Pt(II) species generally show higher oscillator strengths than the corresponding transitions in the *cis* isomers, as observed for the azobenzenes.

From the spectra of calculated orbital energy levels in the four complexes (**Figure 7e**), the HOMO-LUMO gaps for **M1** are relatively larger than those of the *para*-substituted analogues **M2**, at 3.14/3.41 and 2.87/2.99 eV for the *trans*/*cis*-azo geometries, respectively. This appears to be mainly due to a stabilization of the HOMO in the *para* compounds. The larger gaps of the *cis* isomers compared to the *trans* configurations are in both systems due to higher-energy LUMOs.

In the spectrum of *trans*-**M1** complex, the HOMO -> LUMO excitation gives rise to a weak absorption centered around 460 nm. The same excitation gives rise to a relatively much more intense absorption at a slightly red-shifted wavelength of 472 nm in the *trans*-**M2** spectrum. A comparison of the frontier orbitals of *trans*-**M1**/**M2** (**Figures 7f** and **7g**) shows a higher degree of electronic delocalization in the frontier orbitals of the latter complex, particularly the LUMO, suggesting that the enhanced oscillator strength arises from a greater spatial overlap between the frontier orbitals. This explains the much stronger long-wavelength absorption features in the spectra of **M2** and **M3** (see **Figure 3**), both of which incorporate *para*-alkyne azobenzene spacers, compared to that in the spectrum of **M1**, in which the spacer has the Pt-coordinating alkyne groups in the *meta* position.

The strong primary absorption band at 339 nm in the *trans*-**M1** spectrum corresponds to an excitation between the HOMO-9 to the LUMO orbitals, the former of which has electron density delocalized over the azobenzene spacer and the two Pt centers.

The calculations indicate the shorter-wavelength features in the spectra to be composed of multiple transitions, with contributions from a number of occupied and virtual orbitals. We should also note that the larger discrepancy between experiment and theory in this part of the spectrum is due to our including only the first 50 singlet excited states in the simulation of the spectra. However, the present calculations are sufficient to assign and interpret the longer-wavelength absorption features, which are of primary interest here.

CONCLUSIONS

A series of Pt(II) di-ynes and poly-ynes with *meta*- and *para*-substituted azobenzene spacers have been successfully synthesized using a palladium/CuI-catalysed Sonogashira coupling.

From a comprehensive spectroscopic investigation coupled with structural characterization of two model compounds, we have obtained valuable insight into the structure-property relationships for the different azobenzene substitution patterns. Photoisomerisation measurements indicate that the acetylide-functionalised azobenzene ligands and, to a limited extent, the dinuclear and polymeric Pt(II) species incorporating them, can undergo reversible *cis*-*trans* isomerisation under irradiation at UV wavelengths. From spectroscopic measurements and computational modelling, the *trans* geometry about the azo group is confirmed to be the most stable configuration for both the bare ligands and the Pt(II) complexes, with the *cis* isomer of the *para*-alkynyl azobenzene being energetically destabilised by bulky substituents and incorporation into Pt complexes/polymers. A comprehensive analysis of the optical properties using time-dependent density-functional theory calculations has allowed us to characterise the major features in the absorption profiles of the materials, and to interpret them in terms of the underlying electronic structure.

We expect the results from this systematic study to be a valuable addition to the growing body of work on molecular switches, providing insight to aid the future development of functional materials with tunable optical and electronic properties.

ACKNOWLEDGEMENTS

MSK thanks The Research Council (TRC), Oman (Grant No. ORG/EI/SQU/13/015) and His Majesty's Trust Fund for Strategic Research (Grant No. SR/SQU/SCI/CHEM/16/02) for funding. RAB acknowledge SQU for a PhD scholarship, AH acknowledges TRC for a post-doctoral fellowship, and MJ for a PhD scholarship. JMS and PRR are supported by an EPSRC programme grant (grant no. EP/K004956/1). The computational modelling was carried out using the UK Archer facility, accessed through the UK Materials Chemistry Consortium, which is funded by the EPSRC (grant no. EP/L000202). Some modelling was also performed using the Balena HPC system at the University of Bath, which is maintained by Bath University Computing Services.

EXPERIMENTAL

General procedures

All reactions were performed under a dry Ar atmosphere using standard Schlenk line techniques. Solvents were pre-dried and distilled before use according to standard procedures.[31] All chemicals, except where stated otherwise, were obtained from Sigma Aldrich and used as received. The compounds 2,5-dioctyl-4-iodoaniline,[32] 1,2-bis(3-iodophenyl)diazene,[33] 1,2-bis(4-iodophenyl)diazene,[33] bis(4-iodo-2,5-dioctylphenyl)diazene,[33] *trans*-[Ph(Et_3P)$_2$PtCl][34] and *trans*-[(^{n}Bu_3P)$_2$$PtCl_2$][34] were prepared according to reported procedures.

Column chromatography was performed either with Kieselgel 60 (230-400 mesh) silica gel or alumina (Brockman Grade II-III).

NMR spectra were recorded in $CDCl_3$ on Bruker WM-250, WM-300 or AM-400 spectrometers, or on a Bruker Avance III HD 700 MHz spectrometer equipped with 5mm TCI H/C/N cryoprobe. The ^{1}H and ^{13}C NMR spectra were referenced to solvent resonances, and ^{31}P NMR spectra were referenced to external 85% H_3PO_4 (^{31}P{^{1}H}) for **M1**, **M2**, **P1** and **P2** or PPh_3 (for **M3** and **P3**. Attenuated total-reflectance (ATR) infrared (IR) spectra were recorded on pure samples on diamond using a Cary 630 FT-IR spectrometer. Mass spectra were obtained using a VG Autospec magnetic sector instrument using electrospray ionization (ESI).

Absorption spectra were recorded on a Varian-Cary 50 UV-visible spectrophotometer using a quartz cuvette with a 1 cm path length. The photo-irradiation experiments were carried out in toluene/DCM under a multiband UV lamp (UVGL – 55, Mineralight Lamp, 230 V, 6W). This type of lamp emits radiation at both short (254 nm) and longer (365 nm) wavelengths; the shorter-wavelength window was used for these experiments. Spectra were recorded at intervals of 10 mins.

The molar masses of the Pt(II) poly-ynes were determined by gel-permeation chromatography/light-scattering (GPC/LS) analysis. GPC[29] was carried out using two PL Gel 30 cm, 5 micron mixed C columns at 30 °C, running in THF at 1 cm^3 min^{-1} with a Roth Model 200 high-precision pump. This was coupled to a DAWN DSP Wyatt Technology multiangle laser light-scattering (MALLS) apparatus with 18 detectors and an auxiliary Viscotek model 200 differential refractometer/viscometer, which were used to calculate the molecular weights.

Microanalyses were performed at the University Chemical Laboratory, University of Cambridge. Elemental analysis for carbon, hydrogen and nitrogen was performed using a Perkin Elmer 2400 CHNS/O Series II Elemental Analyser.

Caution! All chemicals used in the current work are irritants to skin, eyes and the respiratory system. Therefore, all reactions were performed in well-ventilated fume hood. Inhalation of silica/alumina and low boiling point solvents like dichloromethane and hexane may cause injuries to internal organs. Safety glasses, gloves, masks and lab coats were worn during the experiments.

Ligand synthesis

***1,2-Bis(3-(2-(trimethylsilyl)ethynyl)phenyl)diazene,* 1a**

To a solution of 1,2-bis(3-iodophenyl)diazene (2.00 g, 4.61 mmol) in $^{i}Pr_2NH$/THF (120 cm^3, 1:4 v/v) under an Ar atmosphere was added catalytic amounts of CuI (10 mg), $Pd(OAc)_2$ (10 mg) and PPh_3 (60 mg). The solution was stirred for 30 mins at room temperature followed by addition of trimethylsilylethyne (1.64 mL, 11.5 mmol) with vigorous stirring. The reaction mixture was then refluxed overnight. The completion of the reaction was confirmed by silica TLC and IR spectroscopy. After being cooled to room temperature, the mixture was quenched with water (60 mL) and extracted with CH_2Cl_2 (60 x 2 mL). The organic layer was collected and dried over $MgSO_4$, filtered and the solvent removed under reduced pressure. The solid residue was re-dissolved in CH_2Cl_2 and purified by silica column chromatography, eluting with hexane/CH_2Cl_2 (1: 1 v/v) to obtain the title compound as an orange solid (1.41 g, 81.4 % yield, m. p. 120.5 ºC). IR (CH_2Cl_2): ν/cm^{-1} 2155 (C≡C). ^{1}H NMR (700 MHz, $CDCl_3$): δ/ppm 8.01 (s, 2 H, H-2, 2'), 7.87 (d, 2 H, *J* = 8.0 Hz, H-6, 6'), 7.57 (d, 2 H, *J* = 7.7 Hz, H-4, 4'), 7.46 (t, 2 H, *J* = 7.8 Hz, H-5, 5'), 0.27 (s, 18 H, $SiMe_3$). ^{13}C NMR (176 MHz, $CDCl_3$): δ/ppm 153.03 (C-1, 1'), 134.43, 131.13 (C-2, 2', 6, 6'), 129.12, 126.09, 124.28 (C-3, 3', 5, 5'), 104.21, 103.76, 95.91, 95.34 (C≡C), 0.42 ($SiMe_3$). ESI-MS: *m*/z 375.0 (M^+). Anal. calc. for $C_{22}H_{26}N_2Si_2$: C - 70.53 %, H - 7.00 %, N - 7.48 %, found: C 70.62 %, H - 7.07 %., N - 7.43 %.

***1,2-Bis(4-(2-(trimethylsilyl)ethynyl)phenyl)diazene,* 2a**

This compound was synthesized in a manner similar to **1a** using 1,2-bis(4-iodophenyl)diazene to afford the product as an orange-brown solid (77.5 % yield, m. p. 184.5 ºC). IR (CH_2Cl_2): ν/cm^{-1} 2155 (C≡C). ^{1}H NMR (700 MHz, $CDCl_3$): δ/ppm 7.87 (d, 4 H, *J*

= 7.9 Hz, H-2, 6, 2', 6'), 7.57 (d, 4 H, *J* = 7.6 Hz, H-3, 5, 3', 5'), 0.07 (s, 18 H, $SiMe_3$). ^{13}C NMR (176 MHz, $CDCl_3$): δ/ppm 152.31 (C-1, 1'), 129.18, 128.71 (C-2, 2', 6, 6'), 124.33, 123.65 (C-3, 3', 5, 5'), 104.26, 95.39 (C≡C), 0.05 ($SiMe_3$). ESI-MS *m*/z 374.9 (M^+). Anal. calc. for $C_{22}H_{26}N_2Si_2$: C - 70.53 %, H - 7.00 % , N - 7.48 %, found: C 70.42 %, H - 7.01 %., N - 7.41 %.

***Bis(4-trimethylsilylethynyl-2,5-dioctylphenyl)diazene*, 3a**

This compound was synthesized in a manner similar to **1a** using bis(4-iodo-2,5-dioctylphenyl)diazene to afford the product as an orange-brown solid (76.1 % yield). IR (CH_2Cl_2): ν/cm^{-1} 2152 (C≡C). ^1H NMR (700 MHz, $CDCl_3$): δ/ppm 7.42 (s, 2 H, H-6, 6'), 7.41 (s, 2 H, H-3, 3'), 3.05 (t, 4 H, *J* = 7.0 Hz, methylene), 2.76 (t, 4 H, 7.0 Hz, methylene), 1.66−1.21 (m, 48 H, methylene), 0.88-0.84 (m, 12 H, methyl), 0.085 (s, 18 H, $SiMe_3$).^{13}C NMR (176 MHz, $CDCl_3$): δ/ppm 150.13 (C-1, 1'), 143.68 (C-3, 3'), 140.35 (C-5, 5'), 134.42 (C-2, 2'), 124.95 (C-6, 6'), 115.30 (C-4, 4'), 104.05, 100.03 (C≡C), 34.56, 32.29, 31.92, 31.00, 30.96, 30.54, 29.65, 29.54, 29.51, 29.36, 22.70 (methylene), 14.11 (methyl), 1.04 ($SiMe_3$). ES-MS: *m*/z 823.5 (M^+). Anal. calc. for $C_{54}H_{90}N_2Si_2$: C - 78.76 %, H - 11.02 %, N - 3.40 %, found: C 78.72 %, H - 11.11 %., N - 3.36 %.

***1,2-Bis(3-ethynylphenyl)diazene*, 1b**

1a (0.400 g, 1.07 mmol) was proto-desilylated in THF/methanol (20 mL, 4:1 v/v) using aqueous KOH (0.180 g, 3.21 mmol). The reaction mixture was stirred at room temperature for 2 h, after which time TLC and IR revealed that all protected compound had been converted to the terminal dialkyne ligand. The solvent mixture was then removed and the residue dissolved in CH_2Cl_2 and purified by column chromatography on silica using hexane/CH_2Cl_2 (1:1 v/v) as eluent, affording **1b** as a pale orange powder (0.225 g, 91.3 % yield). IR (CH_2Cl_2): ν/cm^{-1} 2109 (C≡C), 3299 (C≡C-H). ^1H NMR (400 MHz, $CDCl_3$): δ/ppm 8.09 (s, 2 H, H-2, 2'), 7.91 (dd, 2 H, *J* = 7.1, 15.3 Hz, H-6, 6'), 7.62 (dd, 2 H, *J* = 7.6, 15.8 Hz, H-4, 4'), 7.43 (m, 2 H, H-5, 5'), 3.06 (s, 2 H, C≡C-H). ^{13}C NMR (100.6 MHz, $CDCl_3$): δ/ppm 152.30 (C-1, 1'), 134.54, 132.13 (C-2, 2', 6, 6'), 128.7, 127.97, 123.65, 122.59 (C-3, 3', 5, 5'), 82.4, 79.9 (C≡C). ESI-MS: *m*/z 231.1 (M^+). Anal. calc. for $C_{16}H_{10}N_2$: C - 83.46 %, H - 4.38 %, N - 12.17 %, found: C 83.52 %, H - 4.41 %., N - 12.09 %.

***1,2-Bis(4-ethynylphenyl)diazene*, 2b**

A similar procedure was followed as in the synthesis of **1b** using **2a** to afford the product as a pale brown powder (88.2 % yield). IR (CH_2Cl_2): ν/cm^{-1} 2106 (C≡C), 3294 (C≡C-H). ^{1}H NMR (400 MHz, $CDCl_3$): δ/ppm 7.90 (dd, 4 H, *J* = 7.3, 15.0 Hz, H-2, 6, 2', 6'), 7.60−7.64 (m, 4 H, H-3, 5, 3', 5'), 3.06 (s, 2 H, C≡C-H). ^{13}C NMR (100.6 MHz, $CDCl_3$): δ/ppm 152.4 (C-1, 1'), 132.6 (C-2, 2', 6, 6'), 124.9 (C-4, 4'), 122.6 (C-3, 3', 5, 5'), 82.4, 79.9 (C≡C). ESI-MS: *m*/z 230.9 (M^+). Anal. calc. for $C_{16}H_{10}N_2$: C - 83.46 %, H - 4.38 %, N - 12.17 %, found: C 83.42 %, H - 4.31 %., N - 12.26 %.

***Bis(4-ethynyl-2,5-dioctylphenyl)diazene*, 3b**

A similar procedure as used in the synthesis of **1b** using **3a** was followed to obtain **3b** as a brown powder (75.6 % yield). IR (CH_2Cl_2): ν/cm^{-1} 2105 (C≡C), 3302 (C≡C-H). ^{1}H NMR (700 MHz, $CDCl_3$): δ/ppm 7.46 (s, 2 H, H-6, 6'), 7.43 (s, 2 H, H-3, 3'), 3.37 (s, 2 H, C≡C-H), 3.07 (t, 4 H, *J* = 7.0, 14.0 Hz, methylene), 2.79 (t, 4 H, *J* = 7.0 Hz, methylene), 1.67 (p, 4 H, *J* = 7.0, 14.0 Hz, methylene), 1.36 (p, 4 H, *J* = 7.0, 14.0 Hz, methylene), 1.32−1.22 (m, 40 H, methylene), 0.87−0.85 (m, 12 H, methyl). ^{13}C NMR (176 MHz, $CDCl_3$): δ/ppm 150.31, 143.70, 140.30, 134.93, 124.00, 115.32 (aromatic C), 82.43, 82.34 (C≡C), 34.23, 34.19, 31.92, 31.90, 29.71, 29.62, 29.49, 29.45, 29.34, 29.28, 29.23 (methylene), 14.11, 14.09 (methyl). ESI-MS: *m*/z 679.6 (M^+). Anal. calc. for $C_{48}H_{74}N_2$: C - 84.89 %, H - 10.98 %, N - 4.12 %, found: C 84.79 %, H - 10.91 %., N - 4.16 %.

Synthesis of Pt(II)) di-ynes and poly-ynes

***Trans-[(Ph)(Et$_3$P)$_2$Pt-C≡C-R-C≡C-Pt(PEt$_3$)$_2$(Ph)] (R = diphenyldiazene-3,3`-diyl),* M1**

To a stirred mixture of **1b** (0.0500 g, 0.217 mmol) and *trans*-[$Pt(PEt_3)_2PhCl$] (0.236 g, 0.434 mmol) in ^{i}Pr$_2$NH (3 mL) and CH_2Cl_2 (20 mL) was added CuI (0.5 mg). The solution was stirred at room temperature under an Ar atmosphere over a period of 18 h, after which all volatile components were removed under reduced pressure. The crude product was taken up in CH_2Cl_2 and passed through a silica column with hexane/CH_2Cl_2 (1:1 v/v) as eluent. The product was obtained as a yellow solid (0.164 g, 60.7 % yield, m. p. 173.9 ºC). IR (CH_2Cl_2): ν/cm^{-1} 2093 (C≡C). ^{1}H NMR (700 MHz, $CDCl_3$): δ/ppm 7.83 (s, 2 H, H-2, 2'), 7.64−7.62 (m, 2 H, H-6, 6'), 7.39 (d, 2 H, *J* = 7.6 Hz, H-4, 4'), 7.36−7.26 (m, 2 H, H-5, 5'), 7.06 (d, 4 H, *J* = 7.7 Hz, H_{ortho} of Ph), 6.99−6.95 (m, 4 H, H_{meta} of Ph), 6.81 (t, 2 H, *J* = 6.9 Hz, H_{para} of Ph) 1.80−1.08 (m, 24 H, P-CH_2), 1.13−1.06 (m, 36 H, methyl). ^{13}C NMR (176 MHz, $CDCl_3$):

δ/ppm 152.98, 152.65 (C-1, 1'), 139.15, 139.09 (C-4, 4'), 130.88, 130.27, 130.09, 129.81 (C of Ph), 128.80, 128.45 (C-5, 5``), 123.89 (C-6, 6'), 109.58, 109.24 (C≡C), 38.72, 31.92, 30.35, 29.96, 28.92, 23.73, 22.98, 22.69 (methylene), 15.19, 15.10, 15.06, 15.00, 14.12, 14.05 (methyl). $^{31}P\{^{1}H\}$-NMR (400 MHz, $CDCl_3$): δ/ppm 9.97, $^{1}J_{Pt\text{-}P}$ = 2653.78 Hz. ESI-MS: *m*/z 1245.4 (M^+). Anal. calc. for $C_{52}H_{78}N_2P_4Pt_2$: C - 50.16 %, H - 6.31 %, N - 2.25 %, found: C – 50.18 %, H - 6.37 %., N - 2.29 %.

Trans-[(Ph)(Et$_3$P)$_2$Pt-C≡C-R-C≡C-Pt(PEt$_3$)$_2$(Ph)] (R = diphenyldiazene-4,4`-diyl), **M2**

A similar procedure as for the synthesis of **M1** was followed using **2b**. The product was obtained as an orange solid (62.4 % yield, m. p. 190.2 ºC). IR (CH_2Cl_2): ν/cm^{-1} 2090 (C≡C). ^{1}H NMR (700 MHz, $CDCl_3$): δ/ppm 7.77 (d, 4 H, *J* = 8.4 Hz, H-2, 6, 2', 6'), 7.38 (d, 4 H, *J* = 9.1 Hz, H-3, 5, 3', 5'), 7.33 (d, 4 H, *J* = 7.0 Hz, H_{ortho} of Ph), 6.975 (t, 4 H, *J* = 7.4 Hz, H_{meta} of Ph), 6.92 (t, 2 H, *J* = 7.5 Hz, H_{para} of Ph), 1.77 (m, 24 H, P-CH_2), 1.08 (m, 36 H, methyl). ^{13}C NMR (176 MHz, $CDCl_3$): δ/ppm 150.03 (C-1, 1'), 139.25 (C-2, 6, 2', 6'), 136.93 (C-3, 5, 3', 5'), 131.60 (C-4, 4'), 128.01, 127.49, 122.78, 122.03, 121.47 (C of Ph), 111.33 (C≡C), 40.12, 33.52, 31.20, 29.59, 29.01, 25.46, 23.90, 23.16 (methylene), 15.44, 15.34, 15.24, 15.14, 13.55 (methyl). $^{31}P\{^{1}H\}$-NMR (400 MHz, $CDCl_3$): δ/ppm 10.07, $^{1}J_{Pt\text{-}P}$ = 2648.57 Hz. ESI-MS: *m*/z 1245.6 (M^+) Anal. calc. for $C_{52}H_{78}N_2P_4Pt_2$: C - 50.16 %, H - 6.31 %, N - 2.25 %, found: C – 50.12 %, H - 6.29 %., N - 2.31 %.

Trans-[(Ph)(Et$_3$P)$_2$Pt-C≡C-R-C≡C-Pt(PEt$_3$)$_2$(Ph)] (R = 2,5-dioctyldiphenyldiazene-4,4`-diyl), **M3**

A Similar procedure was followed as for the synthesis of **M1** using **3b**. The product was obtained as an orange viscous liquid (61.3 % yield). IR (CH_2Cl_2): ν/cm^{-1} 2095 (C≡C). ^{1}H NMR (700 MHz, $CDCl_3$): δ/ppm 7.47 (s, 4 H, 3, 6, 3', 6'), 7.35 (d, 4 H, *J* = 7.0 Hz, H_{ortho} of Ph), 6.97 (t, 4 H, *J* = 7.4 Hz, H_{meta} of Ph), 6.81 (t, 2 H, *J* = 7.2 Hz, H_{para} of Ph), 3.05 (t, 8 H, *J* = 7.0 Hz, methylene), 2.83 (t, 24 H, *J* = 7.0 Hz, P-CH_2), 1.82−1.64 (m, 8 H, methylene), 1.44−1.36 (m, 24 H, methylene), 1.35−1.20 (m, 16 H, methylene), 1.14−1.06 (m, 12 H, methyl), 0.87 (dt, *J* = 7.0, 10.7 Hz, 36 H, methyl). ^{13}C NMR (176 MHz, $CDCl_3$): δ/ppm 147.90, 141.08, 139.80, 139.26, 133.31, 131.07, 127.33, 121.23 (aromatic C), 114.74, 110.04 (C≡C), 34.67, 32.42, 32.04, 32.00, 31.36, 30.54, 29.98, 29.88, 29.85, 29.73, 29.64, 29.50, 29.48, 22.76, 22.74 (methylene), 15.29, 15.19, 15.09, 14.15 (methyl). $^{31}P\{^{1}H\}$ NMR (121.5 MHz, $CDCl_3$): δ/ppm 9.38, $^{1}J_{Pt\text{-}P}$ = 2629.3 Hz. ESI-MS: *m*/z 1695.3 (M^+). Anal. calc. for

$C_{84}H_{142}N_2P_4Pt_2$: C - 59.55 %, H - 8.45 %, N - 1.65 %, found: C – 59.52 %, H - 8.51 %., N - 1.66 %.

Trans- [-(Bu$_3$P)$_2$Pt -C≡C-R-C≡C-]$_n$, (R = diphenyldiazene-3,3`-diyl), **P1**

P1 was synthesized by mixing **1b** (0.0500 g, 0.217 mmol), *trans*-[Pt(PBu$_3$)$_2$Cl$_2$] (0.146 g, 0.217 mmol) and CuI (0.5 mg) in ^{i}Pr$_2$NH/CH$_2$Cl$_2$ (20 mL, 1:1 v/v). After stirring at room temperature overnight under Ar, the solution mixture was evaporated to dryness. The residue was dissolved in CH$_2$Cl$_2$ and filtered through a short alumina column using hexane/CH$_2$Cl$_2$ (1:1 v/v) as eluent to remove ionic impurities and residual catalyst. After removal of the solvent, the crude product was purified twice by precipitation from MeOH in CH$_2$Cl$_2$. Subsequent washing with hexane and drying under reduced pressure gave an orange solid as product (0.114 g, 80.0 % yield; m. p. 139.8 ºC). IR (CH$_2$Cl$_2$): ν/cm^{-1} 2098 (C≡C). ^{1}H NMR (700 MHz, CDCl$_3$): δ/ppm 8.22 (s, 2 H, H-2, 2’), 7.88 (d, 2 H, *J* = 8.2 Hz, H-6, 6’), 7.84−7.75 (m, 2 H, H-4, 4’), 7.70−7.60 (m, 2 H, H-5, 5’), 2.22−1.96 (m, 12 H, P-CH$_2$), 1.69−1.56 (m, 24 H, methylene), 0.98–0.80 (m, 18 H, methyl). ^{13}C NMR (176 MHz, CDCl$_3$): δ/ppm 152.73, 152.33 (C-1, 1’), 133.87, 133.27 (C-4, 4’), 130.25, 130.13 (C-5, 5’), 128.75, 128.61 (C-2, 2’), 124.89, 123.57 (C-3, 3’), 120.23, 119.90 (C-6, 6’), 110.68 (C≡C), 26.55, 26.52, 26.25, 25.94, 24.61, 24.57, 24.54, 24.47, 24.44, 24.23, 24.18, 24.13, 24.08, 24.03, 22.15 (methylene), 14.02, 13.98 (methyl). ^{31}P{^{1}H} NMR (500 MHz, CDCl$_3$): δ/ppm 3.27, $^{1}J_{Pt\text{-}P}$ = 2346.70 Hz. Anal. calc. for [C$_{40}$H$_{62}$P$_2$N$_2$Pt]$_n$: C - 57.96 %, H - 7.66 %., N - 3.38 %; found: C – 58.12 %, H - 7.51 %., N - 3.36 %. GPC (THF): $\bar{M}_n$ = 29500 gmol^{-1} (*n* = 36), $\bar{M}_w$ = 41800 gmol^{-1}, PDI = 1.4.

Trans- [-(Bu$_3$P)$_2$Pt -C≡C-R-C≡C-]$_n$, (R = diphenyldiazene-4,4`-diyl), **P2**

P2 was synthesized by following the same procedure as for **P1** using **2b**. The title compound was obtained as an orange solid (78.3 %, decomposition temp. 211.5 ºC) . IR (CH$_2$Cl$_2$): ν/cm^{-1} 2097 (C≡C). ^{1}H NMR (700 MHz, CDCl$_3$): δ/ppm 7.81−7.74 (m, 4 H, H-2, 6, 2’, 6’), 7.40−7.32 (m, 4 H, H-3, 5, 3’,5’), 2.13 (t, *J* = 7.2 Hz, 12 H, P-CH$_2$), 1.63 (dd, *J* = 3.4, 7.0 Hz, 12 H, methylene), 1.47 (dq, 12 H, *J* = 7.3, 14.5 Hz, methylene), 0.94 (t, *J* = 7.2 Hz, 18 H, methyl).^{13}C NMR (176 MHz, CDCl$_3$): δ/ppm 152.4 (C-1, 1’), 133.11 (C-2, 6, 2’, 6’), 132.18 (C-3, 5, 3’, 5’), 122.53 (C-4, 4’), 111.40 (C≡C), 29.84, 26.74, 26.74, 26.53, 24.72, 24.68, 24.60, 24.56, 24.53, 24.22, 24.13, 24.03 (methylene), 13.98 (methy l). ^{31}P{^{1}H} NMR (500 MHz, CDCl$_3$): δ/ppm 3.31, $^{1}J_{Pt\text{-}P}$ = 2337.50 Hz. Anal. calc. for [C$_{72}$H$_{62}$P$_2$N$_2$Pt]$_n$: C - 57.96

%, H - 7.66 %, N – 3.38 %; found: C – 58.17 %, H - 7.52 %, N - 3.34 %. GPC (THF): $\bar{M}_n$ = 28800 gmol^{-1} (n = 35), $\bar{M}_w$ = 50500 gmol^{-1}, PDI = 1.3.

Trans- [-(Bu$_3$P)$_2$Pt -C≡C-R-C≡C-]$_n$, (R = 2,5-dioctyldiphenyldiazene-4,4`-diyl), **P3**

P3 was synthesized by following the procedure as for **P1** using **3b** to afford the product as a dark orange solid (79.3 %). IR (CH_2Cl_2): ν/cm^{-1} 2095 (C≡C). ^{1}H NMR (700 MHz, $CDCl_3$): δ/ppm 7.41 (s, 2 H, H-6, 6'), 7.39 (s, 2 H, H-3, 3'), 3.04−2.60 (m, 8 H, methylene), 2.79−2.69 (m, 12 H, P-CH_2), 1.68−1.44 (m, 48 H, methylene), 1.43−1.10 (m, 24 H, methylene), 0.92−0.74 (m, 30 H, methyl). ^{13}C NMR (176 MHz, $CDCl_3$): δ/ppm 148.11, 141.03, 139.96, 133.58, 130.97, 127.64 (aromatic C), 114.78 (C≡C), 34.59, 32.62, 32.18, 32.13, 31.48, 30.48, 30.03, 29.86, 29.79, 29.65, 29.58, 26.60, 26.53, 26.30, 24.61, 24.57, 24.53, 24.41, 24.19, 24.09, 24.00, 22.88, 22.18 (methylene), 14.28, 14.07, 14.02 (methyl). ^{31}P{^{1}H} NMR (121.5 MHz, $CDCl_3$): δ/ppm 2.76, $^1J_{Pt\text{-}P}$ = 2341.3 Hz. Anal. calc. for $[C_{40}H_{126}P_2N_2Pt]_n$: C - 67.68 %, H - 10.02 %, N - 2.19 % ; found: C - 67.76 %, H - 9.96 %, N - 2.20 %. GPC (THF): $\bar{M}_n$ = 70200 gmol^{-1} (n = 55), $\bar{M}_w$ = 84400 gmol^{-1}, PDI = 1.2.

X-ray crystallography

Single-crystal X-ray diffraction experiments were performed at 150 K (for **M1**) and 250 K (for **M2**) on an Oxford Diffraction Gemini A Ultra CCD diffractometer using monochromatic Mo-K_α radiation (λ = 0.71073 Å). The sample temperature was controlled using an Oxford Diffraction Cryojet apparatus. CrysAlis Pro was used for the collection of frames of data, indexing reflections and determining lattice parameters. Structures were solved by direct methods using SHELXS-86[35] and refined using full-matrix least-squares on F^2 with SHELX-97[36] (for **M2**) and SHELX2014[37] (for **M1**) within the Olex2 package.[38] A multi-scan absorption correction was applied in for both cases. For **M2** the phosphine ligands were disordered over two sites, and the ethyl groups were refined with partial occupancies summed to unity, and bond parameter restraints were used to maintain chemically sensible geometries for these groups. For both structures hydrogen atoms were included using rigid methyl groups or a riding model and, again, partial occupancies were used as appropriate. Refinement for both structures continued until convergence was reached, and in the final cycles of refinement a weighting scheme was used that gave a relatively flat analysis of variance.

Computational modelling

Computational modelling was carried out on the azobenzene ligands **1b** and **2b**, together with the corresponding Pt(II) di-ynes **M1** and **M2**, within the density-functional theory (DFT) formalism, as implemented in the NWChem code.[39] We used the B3LYP hybrid functional for all calculations.[40] The electronic wavefunctions were expanded in split-valence Gaussian basis sets of 6-31G and 6-31G** quality for the H and main-group atoms, respectively.[41] The core electrons of the Pt atoms were described by the LANL2DZ effective-core pseudopotential,[42] and the valence electrons were modelled with the corresponding double-zeta basis set. During the electronic-wavefunction minimisation, convergence criteria of 10^{-6}, 10^{-5} and 5×10^{-4} a. u. were applied to the energy, density and gradients, respectively.

Initial models of the *meta*- and *para*-azo Pt(II) systems with the central azobenzenes in the *trans* configuration were extracted from the crystal structures, and models of the corresponding *cis* isomers made by rotating around the central bond. Models of the azobenzene ligands were subsequently prepared from the four Pt complexes. The initial coordinates were optimised until the maximum and root-mean-square (RMS) gradients on the ions were less than 4.5×10^{-4} and 3×10^{-4} a. u., respectively, and the maximum and RMS Cartesian steps in the last iteration fell below 1.8×10^{-3} and 1.2×10^{-3} a. u. The optimised gas-phase structures were confirmed to be stationary points by calculating the nuclear Hessian matrices using analytical gradients. For these calculations, the tolerances on the energy, density and gradients applied during the wavefunction optimisation were tightened, respectively, to 10^{-8}, 10^{-6} and 10^{-5} a. u.

To approximately model the effect of a solvent environment on the energetics and optical absorption spectra, the relaxed structures were further optimised using the COnductor-like Screening MOdel (COSMO)[26] with dielectric constants of ε = 2.38 (toluene), ε = 8.93 (CH_2Cl_2), and ε = 80.1 (H_2O).

The optical properties of the dicholormethane models were studied using time-dependent DFT (TD-DFT) calculations[39] using adiabatic B3LYP, and with a dielectric continuum with ε = 8.93 as in the geometry optimisation. The 50 lowest-energy singlet (spin-allowed) and triplet (spin-forbidden) transitions of each model were computed, and the spin-allowed excitations were used to simulate UV/visible absorption spectra according to:

$$\varepsilon(v) = \sum_i 1.3062974 \times 10^8 \frac{f_i}{\sigma} \exp\left(-\left[\frac{v - v_i}{\sigma}\right]^2\right)$$

where the energies are in cm^{-1}, ε is the molar extinction coefficient in L mol^{-1} cm^{-1}, f_i are the (dimensionless) oscillator strengths, v_i are the band positions and σ is the bandwidth, here set to 0.2 eV.

Supporting information

Supporting Information including UV/visible spectra from photoisomerisation experiments on **1a**/**M1**/**P1** and **2a**/**M2**/**P2** in toluene and orbital assignments of the most intense transitions obtained in the TD-DFT calculations on **1b**, **2b**, **M1** and **M2** is available free of charge on the ACS Publications website at DOI: 10.1021/acs.inorg-chem.xxxxx. The structures are available in CIF format under the CCDC reference numbers **1486091** and **1486092**.

Data-access statement

Crystallographic data from the structural analysis have been deposited with the Cambridge Crystallographic Data Centre under the CCDC codes 1486091 - 1486092, and are available free of charge from https://summary.ccdc.cam.ac.uk/structure-summary-form. Data from the calculations, including the coordinates of the optimised models and simulated spectroscopic data, are available from an online repository at [TODO: URL will be added on acceptance]. Any other data may be obtained on request from the authors.

References:

1. (a) Wong, W.-Y.; Ho, C.-L., Organometallic photovoltaics: a new and versatile approach for harvesting solar energy using conjugated polymetallaynes. *Acc. Chem. Res.* **2010,** *43*, 1246-1256; (b) Xiang, J.; Ho, C.-L.; Wong, W.-Y., Metallopolymers for energy production, storage and conservation. *Polym. Chem.* **2015,** *6*, 6905-6930.
2. García-Amorós, J.; Velasco, D., Recent advances towards azobenzene-based light-driven real-time information-transmitting materials. *Beilstein J. Org. Chem.* **2012,** *8*, 1003-1017.
3. Rau, H., Photoisomerization of azobenzenes. *Photochem. Photophys.* **1990,** *2*, 119-141.
4. (a) Zhang, L.; Cole, J. M.; Dai, C., Variation in optoelectronic properties of azo dye-sensitized TiO2 semiconductor interfaces with different adsorption anchors: carboxylate, sulfonate, hydroxyl and pyridyl groups. *ACS Appl. Mater. Interfaces* **2014,** *6*, 7535-7546; (b) Zhao, Y.; Ikeda, T., *Smart light-responsive materials: azobenzene-containing polymers and liquid crystals*. John Wiley & Sons: 2009.
5. Jura, M.; Raithby, P. R.; Wilson, P. J., In *Molecular Design and Applications of Photofunctional Polymers and Materials*, Wong, W.-Y.; Abd-El-Aziz, A. S.; Weder, C., Eds. Royal Society of Chemistry: Cambridge UK, 2012.

6. Ho, P. K. H.; Kim, J.-S.; Burroughes, J. H.; Becker, H.; Li, S. F. Y.; Brown, T. M.; Cacialli, F.; Friend, R. H., Molecular-scale interface engineering for polymer light-emitting diodes. *Nature* **2000,** *404*, 481-484.
7. Tessler, N.; Denton, G.; Friend, R., Lasing from conjugated-polymer microcavities. *Nature* **1996,** *382*, 695-697.
8. (a) Yu, G.; Gao, J.; Hummelen, J. C.; Wudl, F.; Heeger, A. J., Polymer Photovoltaic Cells: Enhanced Efficiencies via a Network of Internal Donor-Acceptor Heterojunctions. *Science* **1995,** *270*, 1789-1791; (b) Liu, B.; Png, R.-Q.; Zhao, L.-H.; Chua, L.-L.; Friend, R. H.; Ho, P. K. H., High internal quantum efficiency in fullerene solar cells based on crosslinked polymer donor networks. *Nat. Commun.* **2012,** *3*, 1321; (c) Wong, W.-Y.; Wang, X.-Z.; He, Z.; Djurišić, A. B.; Yip, C.-T.; Cheung, K.-Y.; Wang, H.; Mak, C. S.; Chan, W.-K., Metallated conjugated polymers as a new avenue towards high-efficiency polymer solar cells. *Nat. Mater.* **2007,** *6*, 521-527.
9. (a) Garnier, F.; Hajlaoui, R.; Yassar, A.; Srivastava, P., All-polymer field-effect transistor realized by printing techniques. *Science* **1994,** *265*, 1684-1686; (b) Sirringhaus, H.; Tessler, N.; Friend, R. H., Integrated optoelectronic devices based on conjugated polymers. *Science* **1998,** *280*, 1741-1744.
10. Caliendo, C.; Fratoddi, I.; Russo, M. V.; Sterzo, C. L., Response of a Pt-polyyne membrane in surface acoustic wave sensors: Experimental and theoretical approach. *J. Appl. Phys.* **2003,** *93*, 10071-10077.
11. Khan, M. S.; Al-Suti, M. K.; Maharaja, J.; Haque, A.; Al-Balushi, R.; Raithby, P. R., Conjugated poly-ynes and poly (metalla-ynes) incorporating thiophene-based spacers for solar cell (SC) applications. *J. Organomet. Chem.* **2016,** *812*, 13-33.
12. (a) Khan, M. S.; Al-Mandhary, M. R.; Al-Suti, M. K.; Ahrens, B.; Mahon, M. F.; Male, L.; Raithby, P. R.; Boothby, C. E.; Köhler, A., Synthesis, characterisation and optical spectroscopy of diynes and poly-ynes containing derivatised fluorenes in the backbone. *Dalton Trans.* **2003**, 74-84; (b) Khan, M. S.; Al-Mandhary, M. R. A.; Al-Suti, M. K.; Al-Battashi, F. R.; Al-Saadi, S.; Ahrens, B.; Bjernemose, J. K.; Mahon, M. F.; Raithby, P. R.; Younus, M.; Chawdhury, N.; Köhler, A.; Marseglia, E. A.; Tedesco, E.; Feeder, N.; Teat, S. J., Synthesis, characterisation and optical spectroscopy of platinum(II) di-ynes and poly-ynes incorporating condensed aromatic spacers in the backbone. *Dalton. Trans.* **2004,**, 2377-2385; (c) Khan, M. S.; Al-Mandhary, M. R. A.; Al-Suti, M. K.; Corcoran, T. C.; Al-Mahrooqi, Y.; Attfield, J. P.; Feeder, N.; David, W. I. F.; Shankland, K.; Friend, R. H.; Köhler, A.; Marseglia, E. A.; Tedesco, E.; Tang, C. C.; Raithby, P. R.; Collings, J. C.; Roscoe, K. P.; Batsanov, A. S.; Stimson, L. M.; Marder, T. B., Synthesis and optical characterisation of platinum(II) poly-yne polymers incorporating substituted 1,4-diethynylbenzene derivatives and an investigation of the intermolecular interactions in the diethynylbenzene molecular precursors. *New J. Chem.* **2003,** *27*, 140-149; (d) Khan, M. S.; Al-Mandhary, M. R. A.; Al-Suti, M. K.; Feeder, N.; Nahar, S.; Köhler, A.; Friend, R. H.; Wilson, P. J.; Raithby, P. R., Synthesis, characterisation and electronic properties of a series of platinum(II) poly-ynes containing novel thienyl-pyridine linker groups. *J. Chem. Soc., Dalton Trans.* **2002**, 2441-2448; (e) Khan, M. S.; Al-Mandhary, M. R. A.; Al-Suti, M. K.; Hisahm, A. K.; Raithby, P. R.; Ahrens, B.; Mahon, M. F.; Male, L.; Marseglia, E. A.; Tedesco, E.; Friend, R. H.; Köhler, A.; Feeder, N.; Teat, S. J., Structural characterisation of a series of acetylide-functionalised oligopyridines and the synthesis, characterisation and optical spectroscopy of platinum di-ynes and poly-ynes containing oligopyridyl linker groups in the backbone. *J. Chem. Soc., Dalton Trans.* **2002**, 1358-1368; (f) Khan, M. S.; Al-Suti, M. K.; Al-Mandhary, M. R. A.; Ahrens, B.; Bjernemose, J. K.; Mahon, M. F.; Male, L.; Raithby, P. R.; Friend, R. H.; Köhler, A.; Wilson, J. S., Synthesis and characterisation of new acetylide-functionalised aromatic and hetero-aromatic ligands and their dinuclear platinum complexes. *Dalton Trans.* **2003**, 65-73;

(g) Khan, M. S.; Al-Suti, M. K.; Shah, H. H.; Al-Humaimi, S.; Al-Battashi, F. R.; Bjernemose, J. K.; Male, L.; Raithby, P. R.; Zhang, N.; Köhler, A.; Warren, J. E., Synthesis and characterization of platinum(II) di-ynes and poly-ynes incorporating ethylenedioxythiophene (EDOT) spacers in the backbone. *Dalton Trans.* **2011,** *40*, 10174-10183; (h) Köhler, A.; Khan, A. L. T.; Wilson, J. S.; Dosche, C.; Al-Suti, M. K.; Shah, H. H.; Khan, M. S., The role of C-H and C-C stretching modes in the intrinsic non-radiative decay of triplet states in a Pt-containing conjugated phenylene ethynylene. *J. Chem. Phy.* **2012,** *136*, 094905-8; (i) Li, P.; Ahrens, B.; Choi, K.-H.; Khan, M. S.; Raithby, P. R.; Wilson, P. J.; Wong, W.-Y., Metal-metal and ligand-ligand interactions in gold poly-yne systems. *Cryst. Eng. Commun.* **2002,** *4*, 405-412; (j) Li, P.; Ahrens, B.; Feeder, N.; Raithby, P. R.; Teat, S. J.; Khan, M. S., Luminescent digold ethynyl thienothiophene and dithienothiophene complexes; their synthesis and structural characterisation. *Dalton Trans.* **2005**, 874-883; (k) Sudha Devi, L.; Al-Suti, M. K.; Dosche, C.; Khan, M. S.; Friend, R. H.; Köhler, A., Triplet energy transfer in conjugated polymers. I. Experimental investigation of a weakly disordered compound. *Phy. Rev. B* **2008,** *78*, 045210; (l) Sudha Devi, L.; Al-Suti, M. K.; Zhang, N.; Teat, S. J.; Male, L.; Sparkes, H. A.; Raithby, P. R.; Khan, M. S.; Köhler, A., Synthesis and Comparison of the Optical Properties of Platinum(II) Poly-ynes with Fused and Non-Fused Oligothiophenes. *Macromolecules* **2009,** *42*, 1131-1141; (m) Wilson, J. S.; Dhoot, A. S.; Seeley, A. J. A. B.; Khan, M. S.; Kohler, A.; Friend, R. H., Spin-dependent exciton formation in [pi]-conjugated compounds. *Nature* **2001,** *413*, 828-831; (n) Zhang, N.; Hayer, A.; Al-Suti, M. K.; Al-Belushi, R. A.; Khan, M. S.; Köhler, A., The effect of delocalization on the exchange energy in meta- and para-linked Pt-containing carbazole polymers and monomers. *J. Chem. Phy.* **2006,** *124*, 244701.

13. Al-Balushi, R. A.; Haque, A.; Jayapal, M.; Al-Suti, M. K.; Husband, J.; Khan, M. S.; Koentjoro, O. F.; Molloy, K. C.; Skelton, J. M.; Raithby, P. R., Experimental and Theoretical Investigation for the Level of Conjugation in Carbazole-Based Precursors and Their Mono-, Di- and Polynuclear Pt(II) Complexes. *Inorg. Chem.* **2016,** *55*, 6465-6480.

14. Xu, X.-D.; Zhang, J.; Chen, L.-J.; Zhao, X.-L.; Wang, D.-X.; Yang, H.-B., Large-Scale Honeycomb Microstructures Constructed by Platinum Acetylide Gelators through Supramolecular Self-Assembly. *Chemistry - A European Journal* **2012,** *18*, 1659-1667.

15. Sasaki, T.; Tour, J. M., Synthesis of a New Photoreactive Nanovehicle: A Nanoworm. *Org. Lett.* **2008,** *10*, 897-900.

16. Khan, M. S.; Al-Naamani, R. S.; Ahrens, B.; Raithby, P. R., 2, 5-Bis (trimethylsilylethynyl) thieno [3, 2-b] thiophene. *Acta Crystallogr. Sect. E.- Struct. Rep. Online* **2004,** *60*, o1202-o1203.

17. Lambert, J. B.; Shurvell, H. F.; Cooks, R. G., *Introduction to organic spectroscopy*. Macmillan New York: 1987.

18. Manna, J.; John, K. D.; Hopkins, M. D.; Stone, F. G. A.; Robert, W., The Bonding of Metal-Alkynyl Complexes. In *Advances in Organometallic Chemistry*, Academic Press: 1995; Vol. 38, pp 79-154.

19. Zeitouny, J.; Aurisicchio, C.; Bonifazi, D.; De Zorzi, R.; Geremia, S.; Bonini, M.; Palma, C.-A.; Samorì, P.; Listorti, A.; Belbakra, A., Photoinduced structural modifications in multicomponent architectures containing azobenzene moieties as photoswitchable cores. *J. Mater. Chem.* **2009,** *19*, 4715-4724.

20. Gherab, K. N.; Gatri, R.; Hank, Z.; Dick, B.; Kutta, R.-J.; Winter, R.; Luc, J.; Sahraoui, B.; Fillaut, J.-L., Design and photoinduced surface relief grating formation of photoresponsive azobenzene based molecular materials with ruthenium acetylides. *J. Mater. Chem.* **2010,** *20*, 2858-2864.

21. (a) Matharu, A. S.; Jeeva, S.; Ramanujam, P., Liquid crystals for holographic optical data storage. *Chem. Soc. Rev.* **2007,** *36*, 1868-1880; (b) Nalwa, H. S., *Polymeric*

nanostructures and their applications. American Scientific Publishers: 2007; (c) Natansohn, A.; Rochon, P., Photoinduced motions in azo-containing polymers. *Chem. Rev.* **2002,** *102*, 4139-4176.
22. Ikeda, T.; Tsutsumi, O., Optical switching and image storage by means of azobenzene liquid-crystal films. *Science* **1995,** *268*, 1873-1875.
23. Beharry, A. A.; Sadovski, O.; Woolley, G. A., Azobenzene photoswitching without ultraviolet light. *J. Am. Chem. Soc.* **2011,** *133*, 19684-19687.
24. Fehrentz, T.; Schönberger, M.; Trauner, D., Optochemical genetics. *Angew. Chem. Int. Ed.* **2011,** *50*, 12156-12182.
25. Bianchi, A.; Delgado-Pinar, E.; García-España, E.; Giorgi, C.; Pina, F., Highlights of metal ion-based photochemical switches. *Coord. Chem. Rev.* **2014,** *260*, 156-215.
26. Klamt, A.; Schüürmann, G., COSMO: a new approach to dielectric screening in solvents with explicit expressions for the screening energy and its gradient. *J. Chem. Soc., Perkin Trans. 2* **1993**, 799-805.
27. Momma, K.; Izumi, F., VESTA 3 for three-dimensional visualization of crystal, volumetric and morphology data. *J. Appl. Cryst.* **2011,** *44*, 1272-1276.
28. Crecca, C. R.; Roitberg, A. E., Theoretical Study of the Isomerization Mechanism of Azobenzene and Disubstituted Azobenzene Derviatives. *J. Phys. Chem. A* **2006,** *110*, 8188-8203.
29. Yutaka; T.; Mori, I.; Kurihara, M.; Mizutani, J.; Kubo, K.; Furusho, S.; Matsumura, K.; Tamai, N.; Nishihara, H., Synthesis, Characterization, and Photochemical Properties of Azobenzene-Conjugated Ru(II) and Rh(III) Bis(terpyridine) Complexes. *Inorg. Chem.* **2001**, *40*, 4986-4995.
30. Runge, E.; Gross, E. K., Density-functional theory for time-dependent systems. *Phys. Rev. Lett.* **1984,** *52*, 997.
31. Armarego, W. L. F.; Chai, C. L. L., *Purification of Laboratory Chemicals*. 7 ed.; Butterworth-Heinemann: 2013.
32. Izumi, A.; Teraguchi, M.; Nomura, R.; Masuda, T., Synthesis of conjugated polymers with azobenzene moieties in the main chain. *J. Polym. Sci. Part A: Polym. Chem.* **2000,** *38*, 1057-1063.
33. Kauffman, G. B.; Teter, L. A.; Huheey, J. E., Cis- and Trans-Dichlorobis(Tri-n-butylphosphine)Platinum(II). In *Inorganic Syntheses*, John Wiley & Sons, Inc.: 2007; pp 245-249.
34. (a) Charles Jr, E., *Organometallic polymers*. Elsevier: 2012; (b) Takahashi, S.; Morimoto, H.; Murata, E.; Kataoka, S.; Sonogashira, K.; Hagihara, N., Studies on polyyne polymers containing transition metals in the main chain. VII. Synthesis and characterization of palladium-polyyne polymers. *J. Polym. Sci. Polym. Chem. Ed.* **1982,** *20*, 565-573.
35. Sheldrick, G. M., Phase annealing in SHELX-90: direct methods for larger structures. *Acta Crystallogr., Sect. A: Found. Crystallogr.* **1990,** *46*, 467-473.
36. Sheldrick, G. M., A short history of SHELX. *Acta Crystallogr., Sect. A: Found. Crystallogr.* **2008,** *64*, 112-122.
37. Sheldrick, G. M., Crystal structure refinement with SHELXL. *Acta Crystallogr., Sect. C: Struct. Chem.* **2015,** *71*, 3-8.
38. Bourhis, L. J.; Dolomanov, O. V.; Gildea, R. J.; Howard, J. A.; Puschmann, H., The anatomy of a comprehensive constrained, restrained refinement program for the modern computing environment–Olex2 dissected. *Acta Crystallogr. Sect. A: Found. Adv.* **2015,** *71*, 59-75.
39. Valiev, M.; Bylaska, E. J.; Govind, N.; Kowalski, K.; Straatsma, T. P.; Van Dam, H. J. J.; Wang, D.; Nieplocha, J.; Apra, E.; Windus, T. L.; de Jong, W., NWChem: A

comprehensive and scalable open-source solution for large scale molecular simulations. *Comput Phys Commun* **2010,** *181*, 1477-1489.
40. Becke, A. D., A NEW MIXING OF HARTREE-FOCK AND LOCAL DENSITY-FUNCTIONAL THEORIES. *J. Chem. Phys.* **1993,** *98*, 1372-1377.
41. Ditchfield, R.; Hehre, W. J.; Pople, J. A., Self-Consistent Molecular-Orbital Methods. IX. An Extended Gaussian-Type Basis for Molecular-Orbital Studies of Organic Molecules. *J. Chem. Phys.* **1971,** *54*, 724-728.
42. Hay, P. J.; Wadt, W. R., Ab initio effective core potentials for molecular calculations. Potentials for the transition metal atoms Sc to Hg. *J. Chem. Phys.* **1985,** *82*, 270-283.

For Table of Contents Only

Table of Content Graphic

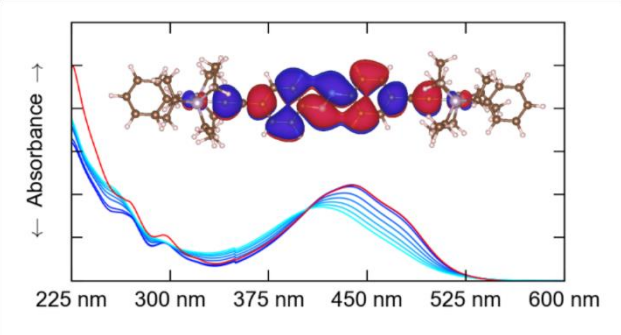

Table of Content Synopsis

The synthesis and characterisation of Pt(II) di- and poly-ynes incorporating *m*- and *p*-alkynyl azobenzene ligands is reported. Combined spectroscopic studies and theoretical modelling reveal limited photoisomerisation and shed light on the degree of electronic delocalisation.